mTORC2 contributes to murine systemic autoimmunity

Xian Zhou[1], Haiyu Qi[1,2], Meilu Li[1,3], Yanfeng Li[1], Xingxing Zhu[1], Shreyasee Amin[1], Mariam Alexander[4], Catherine Diadhiou[5,6], Anne Davidson[5,6], Hu Zeng[1,7]

[1]Division of Rheumatology, Department of Medicine, Mayo Clinic Rochester, MN 55905, USA

[2]Department of Rheumatology, Beijing Friendship Hospital, Capital Medical University, Beijing, 100050, P. R. China

[3]Department of Dermatology, the Second Hospital of Harbin Medical University, Harbin Medical University, Harbin, 150001, P. R. China

[4]Division of Laboratory Medicine and Pathology, Mayo Clinic Rochester, MN 55905, USA

[5]Institute of Molecular Medicine, Feinstein Institutes for Medical Research, Manhasset, NY 11030, USA

[6]Donald and Barbara Zucker School of Medicine at Hofstra/Northwell, Manhasset, NY 11030, USA

[7]Department of Immunology, Mayo Clinic Rochester, MN 55905, USA

Address correspondence and reprint request to Dr. Hu Zeng, Division of Rheumatology, Department of Medicine, Mayo Clinic Rochester, Guggenheim Building 3-42, 200 First ST SW, Rochester, MN, 55902, USA. E-mail address: zeng.hu1@mayo.edu.

Abbreviations used in this article: Tfh, follicular helper T cells; Treg, regulatory T cells; SLE, systemic lupus erythematosus; mTOR, mechanistic target of rapamycin; IFN, interferon; GC, germinal center; EF, extrafollicular; Tfr, follicular regulatory T cells; ICOS, inducible T-cell costimulator.

ABSTRACT

The development of many systemic autoimmune diseases, including systemic lupus erythematosus, is associated with overactivation of the type I interferon (IFN) pathway, lymphopenia, and increased follicular helper T (Tfh) cell differentiation. However, the cellular and molecular mechanisms underlying these immunological perturbations remain incompletely understood. Here we show that the mechanistic target of rapamycin complex 2 (mTORC2) promotes Tfh differentiation and disrupts Treg homeostasis. Inactivation of mTORC2 in total T cells, but not in Tregs, greatly ameliorated the immunopathology in a systemic autoimmunity mouse model. This was associated with reduced Tfh differentiation, B cell activation, and reduced T cell glucose metabolism. Finally, we show that type I IFN can synergize with TCR ligation to activate mTORC2 in T cells, which partially contributes to T cell lymphopenia. These data indicate that mTORC2 may act as downstream of type I IFN, TCR, and costimulatory receptor ICOS, to promote glucose metabolism, Tfh differentiation, and T cell lymphopenia, but not to suppress Treg function in systemic autoimmunity. Our results suggest that mTORC2 might be a rational target for systemic autoimmunity treatment.

INTRODUCTION

The cellular and molecular mechanisms leading to systemic autoimmunity remain poorly understood. A prototype of systemic autoimmunity is systemic lupus erythematosus (SLE). Two major immunological alterations have been identified in lupus, overactivation of the type I IFN signaling pathway and a loss of balance between effector T cells, particularly follicular helper T (Tfh) cells, and regulatory $CD4^+$ T cells (Tregs)[1-3]. Therapeutical options like blocking type I IFN, or its receptor have shown clinical efficacy[4]. Yet, the specific cellular and molecular mechanisms by which type I IFN promotes SLE pathology remain incompletely understood. Recent studies using murine lupus models have demonstrated that type I IFN signaling in $CD4^+$ T cells are required for development of lupus pathology[5,6]. In addition, it is well established that type I IFN can block T cell egress from lymph nodes and induce lymphopenia partly by upregulating the expression of CD69[7,8], a marker that is also associated with lupus pathology[9,10]. Clinical studies[11] and large-scale single cell RNA sequencing analysis[12] confirmed the inverse association between type I IFN activity and the abundance of circulating lymphocytes or naïve $CD4^+$ T cells in SLE patients. However, the type I IFN signaling pathway in $CD4^+$ T cells remains incompletely understood and it is unclear how type I IFN overactivation may be linked to T cell lymphopenia in lupus.

Increased differentiation of Tfh cells has been associated with SLE development and severity in mouse models and human patients[13,14]. Germinal center (GC) Tfh cells, distinguished by expression of the transcription factor BCL6, chemokine receptor CXCR5, and immune checkpoint receptor PD-1, are a specialized effector T cell (Teff) lineage that stimulates B cells in GC to undergo affinity maturation and clonal expansion. The costimulatory receptor ICOS

62 delivers critical signals for Tfh differentiation[15]. In addition, a special subset of Tfh cells with
63 low expression of CXCR5 and P-selectin ligand, PSGL-1, are localized in extrafollicular (EF) to
64 promote generation of plasmablasts, which produce antibodies with modest affinity[16-18]. Both
65 GC and EF responses may contribute to SLE development[19]. In contrast, impaired Treg function
66 is observed in some SLE patients[20]. However, what drives the imbalance between Tfh and Tregs
67 in lupus is not well understood.
68
69 Mechanistic target of rapamycin (mTOR) is a central metabolic pathway, which consists of two
70 complexes, mTORC1 and mTORC2, with scaffolding molecules RAPTOR (encoded by *RPTOR*)
71 and RICTOR (encoded by *RICTOR*) as their defining components, respectively[21]. mTORC1 is
72 critical for naïve T cell quiescence exit and proliferation, and all effector T cells differentiation[22].
73 In contrast, mTORC2 is essential for Tfh differentiation, but dispensable for T cell activation and
74 modestly contributes to other effector T cell lineages[22,23]. Ligation of CD3 and ICOS activates
75 mTORC2, which in turn promotes glucose metabolism in Tfh cells[24]. In terms of Tregs,
76 mTORC1 maintains natural or thymic derived Treg (nTreg, or tTreg) functional competency[25-28].
77 Overactivation mTORC2 impairs Treg suppressive function and stability, especially their ability
78 to suppress Tfh cells, which leads to systemic autoimmune disease with lupus characteristics[29,30].
79 Inhibition of mTORC2 in Tregs can partly restore immune tolerance in the absence of
80 mTORC1[25], or FOXP3[31]. Therefore, mTORC2 signaling controls the balance between Tfh and
81 Treg by promoting the former and suppressing the latter. These fundamental discoveries suggest
82 that targeting mTORC2 in T cells might benefit lupus disease.
83

84 Several studies have examined the contribution of mTORC1 to SLE development[32]. How
85 mTORC2 contributes to systemic autoimmunity has been much less understood. A significant
86 increase of phosphorylation of AKT at serine 473, an established direct target of mTORC2, was
87 observed in T cells from lupus patients and it was associated with disease severity[33,34]. These
88 studies suggest that mTORC2 overactivation might be a potential contributing factor for lupus.
89 The underlying mechanisms, however, remain obscure. Here, we tested the hypothesis that
90 genetic targeting mTORC2 in T cells may improve systemic autoimmunity in C57BL/6-*Fas*^{Lpr}
91 (Lpr) mice. We show that Lpr T cells have an elevated baseline activity of mTORC2. Loss of
92 *Rictor* specifically in T cells significantly improves immunopathology in Lpr mice, including T
93 cell lymphopenia and generation of autoantibodies, which is associated with normalization of the
94 balance between Tfh cells and Tregs. Surprisingly, mTORC2 contributes to systemic
95 autoimmunity primarily through promoting Tfh cells, but not suppressing Tregs, because specific
96 deletion of *Rictor* in Tregs largely fails to ameliorate the immune activation in Lpr mice. Lastly,
97 we demonstrate that type I IFN can synergize with TCR signaling to sustain mTORC2 activation
98 and promote CD69 expression, which suppress T cell egress and lead to lymphopenia, partly in
99 an mTORC2 dependent manner. Our data supports the notion that mTORC2 dependent Tfh
100 expansion, but not Treg impairment, may contribute to the lupus-associated systemic
101 immunopathology.
102
103
104
105
106

107 **MATERIAL and METHODS**

108 **Mice**

109 *Cd4*^{Cre}*Rictor*$^{fl/fl}$ mice have been described before[24]. C57BL/6-*Fas*^{Lpr} and Foxp3^{Cre} mice were

110 purchased from The Jackson Laboratory. Mice were bred and maintained under specific

111 pathogen-free conditions in the Department of Comparative Medicine of Mayo Clinic with

112 IACUC approval.

113 **ELISA**

114 For autoantibodies detection in sera, 96-well plates (2596; Costar) were coated with ssDNA and

115 chromatin (Sigma-Aldrich) in PBS overnight at 4°C used at a concentration of 1.6 μg/ml and 5

116 μg/ml, respectively. Plates were washed twice (0.05% Tween 20 in PBS), blocked with 5%

117 blocking protein (Bio-Rad) for 1 h, and washed twice, and serially diluted sera samples were

118 added for 1.5 h at 37 °C. Plates were washed four times and horseradish peroxidase (HRP)-

119 conjugated detection Abs for IgG (Bethyl Laboratories) were added for 1 h at RT, washed four

120 times, and tetramethylbenzidine (TMB) substrate was added. Reaction was stopped using 2N

121 H_2SO_4 and read at 450 nm. The titers of mouse IgM, IgG, IgG2b and IgG3 (Fig. 1C) in sera were

122 measured with the ELISA kits from Invitrogen.

123 **Mouse immunoglobulin isotyping panel detection**

124 The concentration of mouse immunoglobulin isotypes IgG1, IgG2a, and IgG2b (Fig. 4G) in sera

125 were measured with the LEGENDplex mouse immunoglobulin isotyping panel, according to

126 manufacturer's instructions (Biolegend; cat# 740493).

127 **Immunofluorescence staining**

128 Kidneys were obtained from 6-month-old B6, Lpr and Lpr. *Rictor*$^{fl/fl}$ mice, and fixed in 4%

129 paraformaldehyde (PFA) overnight, osmotically dehydrated in 20 % (w/v) sucrose, embedded in

130 OCT, and cryosectioned to 6 μM. Sections were fixed in −20°C acetone for 2 min and blocked in

131 PBS containing 8% goat serum, 1% bovine serum albumin (BSA) and 0.1% Tween 20 for 45
132 min. Deposition of immunoglobulin (IgG) and complement component 3 (C3) in the kidney
133 tissue were stained with PE labeled goat anti-mouse IgG (Invitrogen) and FITC labeled rat anti-
134 mouse C3 (Cedarlane) antibodies. Similarly, spleens were obtained from 6 months old mice, and
135 processed as above. Frozen sections were fixed and blocked as described above, and incubated
136 with primary antibodies Biotin Peanut Agglutinin (PNA) (Vectorlabs), purified rat anti-mouse
137 CD3 (Biolegend) and PE labeled anti-mouse IgD (BD), or stained with Biotin anti-mouse CD138
138 (Biolegend) and PE labeled anti-mouse IgD at 4°C for 4 hours. Slides were then washed before
139 streptavidin-Alexa Fluor 488 conjugate (ThermoFisher) and Alexa Fluor 647 labeled goat anti-
140 rat secondary antibody (ThermoFisher) were added for 1 h at room temperature. Sections were
141 covered with coverslip and visualized under an Olympus BX51 fluorescence microscope.

142 **Flow cytometry**

143 Single-cell suspension was prepared by passing spleen and peripheral lymph nodes through a 70-
144 µm nylon mesh. For analysis of surface markers, cells were stained in PBS containing 1% (w/v)
145 BSA on ice for 30 min, with APC-labeled anti-ICOS (clone: 7E.17G9; BD), PE-Cy7-labeled anti
146 PD-1 (clone: RMPI-30; BioLegend), Super Bright 600–labeled anti-CD4 (Clone: SK-3;
147 eBioscience), BV510-labeld anti-CD8a (clone:53-6.7; BioLegend); APC-Cy7-labeled TCRβ
148 (clone: H57-597; BioLegend), APC anti-CD162 (PSGL1; clone: 2PH1; BD), BV605-labeled
149 anti-CD25 (clone: PC61; BioLegend), PE-Cy7–labeled anti-CD19 (clone: 6D5; BioLegend),
150 BV605-labeled B220 (clone: RA3-6B2; BioLegend), PE-labeled anti-Fas (clone: Jo2; BD),
151 BV785-labeled anti-CD138 (clone: 281-2; BioLegend), APC-labeled anti-IgD (clone: IA6-2;
152 BioLegend), PerCP-Cyanine5.5-labeled anti-CD38 (clone: 90; BioLegend), FITC-labeled anti-
153 IgG1 (clone: RMG1-1; BioLegend), APC-labeled anti-IL7Rα (clone: SB/199; BioLegend),

154 FITC-labeled anti-CD69 (clone: H1.2F3; Tonbo Bio), PE-labeled anti-CD153 (clone: RM153;
155 eBioscience), PE-labeled anti-CD73 (clone: TY/11.8; BioLegend) and APC-labeled anti-FR4
156 (clone: 12A5; BD). Cell viability was assessed using the Fixable Dye Ghost 540 (Tonbo
157 Bioscience), or 7AAD. CXCR5 and PNA were stained with biotinylated anti-CXCR5 (clone:
158 2G8, BD Biosciences) or biotinylated peanut agglutinin (FL10-71; Vectorlabs), followed by
159 staining with streptavidin-conjugated PE (BD Biosciences). Splenocytes and peripheral lymph
160 node cells were cultured for 4 h at 37°C in complete medium (1640 RPMI + 10% FBS)
161 containing ionomycin (1 μg/ml), PMA (50 ng/ml) and Monensin solution (1,000×; BioLegend)
162 for cytokines detection. Intracellular cytokine staining of IFN-γ (clone: XMG1.2; eBioscience),
163 IL-2 (clone: JES6-5H4; BioLegend) and IL-17A (clone: TC11-18H10.1; BioLegend) were
164 performed using the BD Cytofix/Cytoperm and Perm/Wash buffers or, for transcriptional factors
165 FoxP3 (clone: FJK-16s; eBioscience), Bcl6 (clone: K112-91, BD) and Ki67 (clone: SolA15;
166 eBioscience) staining using the eBioscience Transcription Factor Staining Buffer Set. Phosflow
167 staining for AF647 conjugated phosphor-AKT (S473) (D9E; Cell signaling) was performed
168 using Phosflow Fix/Perm kit (BD Biosciences). Flow cytometry was performed on the Attune
169 NxT (ThermoFisher) cytometer, and analysis was performed using FlowJo software (Tree Star).

170 **Immunoblotting**

171 For immunoblotting, murine $CD4^+$ T cells were isolated from mouse spleen and peripheral
172 lymph node single cell suspension, and human $CD4^+$ T cells were enriched from healthy donor
173 PBMC with STEMCELL mouse or human $CD4^+$ T cell isolation kits, respectively. Cells were
174 lysed in lysis buffer with protease and phosphatase inhibitors (Sigma-Aldrich). Protein
175 concentration in samples was quantified by BCA assay (Thermo Fisher Scientific) before loading
176 the samples for electrophoresis and membrane transfer. The transferred membrane was blocked

177 with TBST (0.1% Tween 20) containing 5% BSA for 1 h at room temperature. The membrane
178 was incubated with primary antibodies overnight including anti-phospho-AKT (Ser473) (clone:
179 D9E; Cell Signaling), AKT (pan) (Clone: 40D4; Cell Signaling), phospho-STAT1 (Tyr701)
180 (clone: D4A7; Cell Signaling), phospho-STAT2 (Tyr690) (Cell Signaling), phospho-S6
181 (Ser235/236) (clone: D57.2.2E; Cell Signaling) and anti-β-actin (clone: 13E5; Sigma-Aldrich).
182 Then, the membrane was washed and incubated with the corresponding secondary antibody for
183 subsequent enhanced chemiluminescence (ECL; Thermo Fisher) exposure. The band intensity of
184 all the immunoblot was analyzed by ImageJ software.

185 **Inflammatory cytokines detection**

186 Murine sera were collected from 6-month-old B6, Lpr and Lpr.*Rictor* T-KO mice. The levels of
187 inflammatory cytokines in serum were measured with the LEGENDplex Multi-Analyte Flow
188 Assay Kit, according to manufacturer's instructions (Biolegend, Mouse Inflammation Panel, cat#
189 740446).

190 **ICOS stimulation**

191 Cell isolation and flow cytometry of lymphocytes were as described. One million $CD4^+$ T cells
192 were activated with plate coated anti-CD3 and anti-CD28 (Bio X Cell). After 2 days activation,
193 T cells were removed from stimulation and rested overnight. Live cells were purified using
194 lymphocyte isolation buffer (MP Biomedicals), followed by stimulation with plate bound anti-
195 CD3 (2 µg/ml) and anti-ICOS (5 µg/ml; C398.4A; Biolegend) for 24 hours.

196 **Metabolic assay**

197 The bioenergetic activities of the OCR and ECAR were measured using a Seahorse XFe96
198 Extracellular Flux Analyzed following established protocols (Agilent). Briefly, equal number of
199 live $CD4^+$ T cells were seeded at 200,000 cells/well on Cell-Tak (Corning) coated XFe96 plate

200 with fresh XF media (Seahorse XF RPMI medium containing 10 mM glucose, 2 mM L-
201 glutamine, and 1 mM sodium pyruvate, PH 7.4; all reagents from Agilent). Basal OCR and
202 ECAR were measured in the presence of Oligomycin (1.5 μM; Sigma-Aldrich), FCCP (1.5 μM;
203 Sigma-Aldrich), and Rotenone (1 μM; Sigma-Aldrich)/ Antimycin A (1 μM; Sigma-Aldrich) in
204 Mito Stress assay. For ECAR measurement in ICOS secondary stimulated $CD4^+$ T cells,
205 glycolytic rate assay was performed according to the manufacturer's manual (Agilent) in
206 presence of Rotenone/Antimycin A and 2-DG (50 mM, Sigma-Aldrich)

207 **Poly(I:C) treatment and cell counting in peripheral blood**

208 *Cd4*^{Cre}*Rictor*$^{fl/fl}$ and wild-type mice were given intraperitoneal injection of 200 μg poly(I:C)
209 (Sigma-Aldrich) in 200 μL PBS, and blood lymphocyte counts were assessed 16 and 40 hours
210 later. Briefly, to determine absolute blood cell counts, 50 μL peripheral blood with 5 μL EDTA
211 was collected, lysed with 1 mL ACK lysing buffer (ThermoFisher), and washed with PBS.
212 Samples were stained with anti-mouse CD19, CD4, CD8 and CD69 antibodies, washed with
213 PBS once, suspended with 500 μL PBS and loaded to Attune NxT cytometer with the accurate
214 acquisition of 250 μL samples. Cell counts were calculated per 5 μL blood.

215 **Statistical Analysis**

216 Statistical analysis was performed using GraphPad Prism (version 8). P values were calculated
217 with Student's *t* test, or one-way ANOVA. $P < 0.05$ was considered significant.

RESULTS

Loss of mTORC2 in T cells improves immunopathology in murine systemic autoimmunity

Lpr mice recapitulate many of the systemic immunoproliferative phenotypes in human lupus disease without developing overt nephritis phenotypes[35]. We tested whether mTORC2 activity is altered in T cells from Lpr mice. Immunoblot analysis showed that $CD4^+$ T cells from Lpr mice had elevated phosphorylation of AKT at Serine 473 (p-AKT_{473}), a direct target of mTORC2, indicating overactivation of mTORC2 in Lpr T cells at baseline (Fig. 1A). To test the hypothesis that targeting mTORC2 may improve systemic autoimmunity, we crossed *Cd4*^{Cre}*Rictor*$^{fl/fl}$ mice, in which *Rictor* is specifically deleted and hence abrogates mTORC2 activity in T cells[24,25], with Lpr mice to generate C57BL/6.*Fas*^{Lpr}*Cd4*^{Cre}*Rictor*$^{fl/fl}$ (Lpr.*Rictor* T-KO) mice. RICTOR deficiency in T cells alone does not significantly impact immune cell homeostasis and overall mouse health[25,36,37]. Therefore, we focused on the comparison among B6, Lpr and Lpr.*Rictor* T-KO mice. *Fas*^{Lpr} mutation drives dramatic lymphoid hyperplasia, including lymphadenopathy. We observed that deletion of *Rictor* in T cells significantly rescued lymphadenopathy phenotypes (Fig. 1B). Consistent with these findings, Lpr mice had increased total IgM and IgG, and isotypes IgG2b and IgG3 immunoglobulin levels (Fig. 1C) and increased anti-ssDNA and anti-chromatin autoantibodies (Fig. 1D), most of which were significantly reduced in Lpr.*Rictor* T-KO mice. Furthermore, we examined IgG and complement deposition in kidneys, which reflects renal involvement in autoimmunity. Lpr mice on B6 background have very mild kidney pathology compared to those on MRL/MpJ background[38]. Consistent with this observation, we observed a mild increase of IgG and complement C3 deposition in kidneys from Lpr mice. Deletion of *Rictor* reduced IgG and C3 deposition in Lpr.*Rictor* T-KO kidney, although the latter did not reach statistical significance (Supplemental Fig. 1A). Thus, inactivation of mTORC2 in T

241 cells substantially attenuates lymphoid hyperplasia, antibody secretion, and renal immune
242 complex deposition in a mouse model of systemic autoimmunity.
243 Consistent with the attenuated lymphoid hyperplasia in Lpr.*Rictor* T-KO mice, the accumulation
244 of the aberrant $B220^{+}TCR\beta^{+}$ cells in Lpr mice was nearly completely reversed in Lpr.*Rictor* T-
245 KO mice (Fig. 1E). Although Lpr.*Rictor* T-KO mice had a significant increase of $B220^{+}TCR\beta^{-}$
246 B cell percentage, the absolute number of this population modestly, but significantly, reduced in
247 Lpr.*Rictor* T-KO mice compared to Lpr mice (Fig. 1E). $B220^{-}TCR\beta^{+}$ T cell percentages were
248 highly reduced in both Lpr and Lpr.*Rictor* T-KO mice, but Lpr mice had an increase of $B220^{-}$
249 $TCR\beta^{+}$ T cell number likely due to the lymphoid hyperplasia, which was also reversed in
250 Lpr.*Rictor* T-KO mice (Fig. 1E). Moreover, the accumulation of $TCR\beta^{+}CD4^{-}CD8^{-}$ DN T cells
251 was substantially restored by *Rictor* deletion (Fig. 1F). Finally, there were elevated, albeit to a
252 widely variable degree, levels of multiple inflammatory cytokines in Lpr mice, such as IFNβ, IL-
253 1β, TNFα and IL-17A, many of which were rectified in Lpr.*Rictor* T-KO mice (Fig. 1G).
254 Therefore, the inactivation of mTORC2 in T cells significantly reverses the abnormal
255 accumulation of T and B cells, production of immunoglobulin and inflammatory cytokine, and
256 restores immune homeostasis in peripheral lymphoid organs of Lpr mice.
257
258 **mTORC2 in T cells promotes B cell hyper-activation**
259 Reflecting the enhanced antibody levels, immunofluorescence staining revealed a dramatic
260 increase of peanut agglutinin (PNA) staining in Lpr mice, suggesting increased GC reaction. The
261 pattern of the PNA staining was variable. Some are dense aggregations like defined GC
262 formation, but others are more diffused without defined boundaries (Fig. 2A). T cell distribution
263 was also disorganized in Lpr lymphoid tissues. Both the increased PNA staining and

264 disorganized T cell distribution were greatly restored by RICTOR deficiency (Fig. 2A). Flow
265 cytometry analysis confirmed these observations. B cells from Lpr mice had highly increased
266 expression of GC B cell marker GL-7, and significant loss of IgD expression, indicating
267 increased B cell activation and class switch (Fig. 2B). Consistent with this notion, Lpr B cells
268 had greatly increased IgG1 expression (Supplemental Fig. 2A). A large proportion of Lpr B cells
269 lost expression of CD38, a NADase with strong immunosuppressive capacity[39], and the loss of
270 which is another characteristic of germinal center B cells (Supplemental Fig. 2A). Because
271 plasmablasts contribute to extrafollicular response, we stained CD138, a marker of plasmablasts.
272 The results showed a markedly increase of CD138 expression in extrafollicular region of Lpr
273 spleens, which was reduced in Lpr.*Rictor* T-KO mice (Fig. 2C). The RICTOR-dependent
274 increase of extrafollicular response in Lpr mice was confirmed with flow cytometry analysis. Lpr
275 mice accumulated large number of cells with modest expression of CD138, and B220^{lo}CD138^{hi}
276 plasmablast/plasma cells, while deletion of *Rictor* in T cells dramatically suppressed the
277 generation of these populations (Fig. 2D). Therefore, mTORC2 activity in T cells is a major
278 contributor to B cell abnormality in Lpr mice. Taken together, our data indicate that inhibition of
279 mTORC2 in T cells attenuates GC and plasmablast formation in Lpr mice.
280

281 **Increased Tfh differentiation in Lpr mice is dependent on mTORC2**

282 Tfh is key for GC formation. Indeed, we observed many T cells in GC of Lpr mice from
283 immunofluorescence staining, presumably Tfh cells (Fig. 2A). This was confirmed by flow
284 cytometry data, which showed a strong increase of BCL6^{+}CXCR5^{hi} GC Tfh and BCL6^{-}CXCR5^{+}
285 pre-Tfh cells in Lpr mice, that was significantly dependent on RICTOR expression (Fig. 3A and
286 Supplemental Fig. 3A for gating strategy). A RICTOR-dependent CXCR5 expression was also

287 found on TCRβ^{+}CD4^{-}CD8^{-} DN T cells (data not shown). Similar observations were found when
288 using other conventional Tfh markers, PD-1 and CXCR5 (Supplemental Fig. 3B). RICTOR
289 deficiency also reduced PSGL-1^{-}CXCR5^{-} EF Tfh cell frequency (Fig. 3B), consistent with the
290 reduction of plasmablast/plasma cells. These results indicated a critical requirement of mTORC2
291 signaling for autoreactive GC and EF Tfh differentiation in Lpr lupus-prone model. Similar
292 rescue effects were observed at different ages (at 3 and 9 months, data not shown). Like SLE
293 patients[14], Lpr mice had highly increased ICOS expression, both on CXCR5^{+} and CXCR5^{-} T
294 cells. Interestingly, deletion of *Rictor* failed to restore ICOS expression (measured by both
295 positive percentages and mean fluorescence intensity), indicating that the reduced Tfh
296 differentiation in Lpr.*Rictor* T-KO mice is not a consequence of reduced ICOS expression (Fig.
297 3C).
298 Treg cells are key for maintaining immune tolerance and preventing autoimmunity.
299 Counterintuitively, in an inflammatory condition, Treg percentage sometimes paradoxically
300 increases. We found that Lpr mice had variable Treg perturbations dependent on anatomic
301 location: while Treg percentages increased the most in spleens and modestly in peripheral lymph
302 nodes (pLN), they trended lower in the gut mucosal site relative to WT B6 mice (Fig. 3D), in a
303 manner consistent with the graded mTORC2 activity, gradually increasing from spleen to pLN,
304 and to gut mucosal site[24]. In all cases, deletion of *Rictor* significantly restored the Treg
305 homeostasis in Lpr mice (Fig. 3D). The magnitude of changes of Treg frequencies in Lpr mice
306 were much smaller than that of Tfh cells, thus the ratio between Tfh and Treg was drastically
307 increased in Lpr mice, suggesting an imbalance between Tfh and Tregs in Lpr mice. Such
308 imbalance was significantly restored by mTORC2 deficiency (Fig. 3E). FOXP3^{+}CXCR5^{+}
309 follicular regulatory T (Tfr) cells are specialized to suppress Tfh cells and GC formation[40].

310 RICTOR deficiency alone does not impact Tfr differentiation[24]. Lpr mice had a highly increased
311 ratio between Tfh and Tfr cells, which was partly restored in Lpr.*Rictor* T-KO mice (Fig. 3E).
312 However, Lpr mice also had significantly increased frequency of $FOXP3^{+}CXCR5^{+}$ Tfr cells
313 compared to B6 control mice, which was also reversed by *Rictor* deletion (Supplemental Fig.
314 3C). Therefore, the data indicate that RICTOR deficiency impacts Tfh/Tfr ratio primarily by
315 reducing Tfh, not increasing Tfr.
316 Furthermore, we found that *Rictor* deficiency did not restore the increased IFNγ expression (Fig.
317 3F) or alter IL-2 and IL-17 expression in $CD4^{+}$ T cells from Lpr mice (Fig. 3F, 3G), or change
318 the expression of lineage transcription factor Tbet and Rorγt (Supplemental Fig. 3D), consistent
319 with our hypothesis that mTORC2 inactivation preferentially affects Tfh differentiation, but not
320 other effector T cell lineages. These data also suggested that Tregs from Lpr.*Rictor* T-KO mice
321 were not able to control the excessive cytokine production in Lpr $CD4^{+}$ T cells, despite
322 normalization of their homeostasis. Finally, the restoration of T cell phenotypes in Lpr.*Rictor* T-
323 KO mice was likely independent of cell proliferation, because $CD4^{+}$ T cells from Lpr.*Rictor* T-
324 KO mice had similarly increased Ki-67^{+} percentage at steady state as those from Lpr mice (Fig.
325 3H). Therefore, our data showed that mTORC2 contributes to the increased GC and EF Tfh cells
326 in Lpr mice, independent of ICOS receptor expression and T cell proliferation.
327

328 **mTORC2 inactivation in Tregs fails to restore immune homeostasis in Lpr mice**

329 The two best described functions of mTORC2 in T cells are promoting Tfh differentiation[24,41]
330 and suppression of Treg function[25,29]. Thus, it is possible the above-described phenotypic
331 improvements in Lpr.*Rictor* T-KO mice (deletion in all T cells) can be partly attributed to
332 enhanced Treg function. To dissect whether mTORC2 contributes to systemic autoimmunity

333 mainly through inhibiting Tregs, promoting Tfh, or both, we generated
334 C57BL/6.*Fas*^{Lpr}*Foxp3*^{Cre}*Rictor*$^{fl/fl}$ (Lpr.*Rictor* Treg-KO) mice, in which *Rictor* was specifically
335 deleted in Treg cells (Supplemental Fig. 4A). Although *Rictor* deficiency in Tregs can boost
336 Treg suppressive function in the absence of mTORC1[25], *Pten*[29] or *Foxp3*[31], it also reduces
337 peripheral Treg frequency compared to WT controls[25]. Lpr.*Rictor* Treg-KO mice also had
338 reduced Treg percentage compared to Lpr mice, although their Treg percentage was similar to
339 Lpr.*Rictor* T-KO mice (Fig. 4A). We compared the immunological phenotypes between Lpr,
340 Lpr.*Rictor* T-KO, and Lpr.Rictor Treg-KO mice. To our surprise, Lpr.*Rictor* Treg-KO mice had
341 equivalent lymphoplasia found in Lpr mice, as illustrated by the lymphadenopathy (Fig. 4B). The
342 expansion of B220^{+}TCRβ^{+} cells was not affected by Treg specific deletion of *Rictor* (Fig. 4C).
343 Similarly, the elevated Tfh, pre-Tfh and GC B cells in Lpr.*Rictor* Treg-KO mice were all at a
344 comparable level as those found in Lpr mice, in sharp contrast to Lpr.*Rictor* T-KO mice (Fig.
345 4D, E). Because of the elevated Tfh frequency, Lpr.*Rictor* Treg-KO mice retained a high Tfh vs
346 Treg ratio similar to that of Lpr mice (Fig. 4F). Quantification of immunoglobulin concentrations
347 revealed that Lpr.*Rictor* Treg-KO mice had highly elevated antibody levels, some of which
348 (including IgG1 and IgG2a) even surpassed those in Lpr mice, whereas Lpr.*Rictor* T-KO mice
349 had significantly reduced IgG2a and IgG2b levels and IgG1 level trending lower (but not
350 significantly) compared to those in Lpr mice (Fig. 4G). These data support the idea that
351 mTORC2-dependent overactivation of Tfh, but not mTORC2-mediated impairment of Treg
352 cells, contributes to the systemic lymphoproliferation in Lpr mice.
353
354 **Inactivation of mTORC2 restores T cell glucose metabolism**

355 Recent studies indicate that lupus development is associated with dysregulation of T cell
356 immunometabolism[42]. mTORC2 is known as one of the key regulators for cell metabolism. We
357 compared the basal respiration and glycolysis of T cells among B6, Lpr and Lpr.*Rictor* T-KO
358 mice at different ages under TCR signaling stimulation. Consistent with recent publications[43,44],
359 T cells from 2 months old Lpr mice had modestly increased basal respiration and glycolysis (Fig.
360 5A, 5B). Strikingly, T cells from 3 and 9 months old Lpr mice had dramatically decreased basal
361 respiration and glycolysis, relative to B6 mice (Fig. 5A, 5B). The opposite metabolic activities
362 between 2 and 3 months old Lpr mice T cells were associated with drastic changes of naive and
363 effector T cell composition at different ages of Lpr mice during lupus development
364 (Supplemental Fig. 5A). Lpr.*Rictor* T-KO mice had much lower levels of basal respiration and
365 glycolysis compared to B6 mice at all ages (Fig. 5A, 5B). The reduced metabolic activity in
366 primary culture of T cells from older Lpr and Lpr.*Rictor* T-KO mice (compared to 2 months old
367 mice) was consistent with reduced T cell proliferation during primary culture (Supplemental Fig.
368 5B). Because anergic T cells are known to have stunted metabolic activity and reduced
369 glycolysis[45,46], we tested whether the reduced metabolism in 6 months old Lpr T cells was
370 associated with increased anergic T cells. Indeed, we found drastically increased anergy
371 ($FR4^{+}CD73^{+}$)[47] markers on Lpr $CD4^{+}$ T cells at steady state, which was mildly reduced in
372 Lpr.*Rictor* T-KO mice (Supplemental Fig. 5C). Costimulatory signaling from ICOS is important
373 to limit T cell anergy[48]. Furthermore, we have previously shown that mTORC2 functioned as
374 downstream of ICOS receptor to promote Tfh differentiation, which could be modeled by
375 restimulating previously activated T cells with anti-CD3/anti-ICOS[24]. Interestingly, Lpr T cells
376 had enhanced proliferation during secondary activation with anti-CD3/anti-ICOS regardless of
377 the ages (Supplemental Fig. 5D, and data not shown), suggesting that re-stimulation from TCR

378 and ICOS signaling not only reversed the proliferation defect, and possibly broke the anergic
379 status, in Lpr T cells, but also promote more accumulation of Lpr T cells relative to WT control.
380 All these defects were not markedly affected by RICTOR deficiency. mTORC2 promotes
381 TCR/ICOS mediated glucose metabolism during Tfh differentiation[24]. Therefore, we examined
382 the T cell glycolysis after anti-CD3/anti-ICOS secondary stimulation. Lpr $CD4^+$ T cells exhibited
383 a significant increase of compensatory glycolytic rate relative to B6 controls, regardless of the
384 ages. *Rictor* deletion substantially reduced both basal and compensatory glycolytic rate in Lpr
385 $CD4^+$ T cells (Fig. 5C). Therefore, mTORC2 contributes to the TCR/ICOS mediated enhanced
386 glycolysis in Lpr T cells without affecting T cell proliferation.

387 **mTORC2 functions downstream of type I IFN to promote CD69 expression and suppress T**
388 **cell egress**

389 Previous studies have identified that type I IFN contributes to the lupus phenotypes in Lpr
390 mice[49,50]. We also observed increased type I IFN in Lpr mouse serum (Fig. 1G). Interestingly, we
391 found that addition of IFNα significantly enhanced anti-CD3/anti-CD28 induced mTORC2
392 target p-AKT_{473}, but not mTORC1 target p-S6, at 6 h stimulation, which was completely
393 dependent on RICTOR (Fig. 6A). IFNα alone could also induced weak p-AKT_{473}, but the
394 combination of anti-CD3/anti-CD28 and IFNα appeared to be the most potent activators of
395 RICTOR dependent p-AKT_{473} (Fig. 6A, 6B). RICTOR deficiency did not markedly affect
396 canonical IFNα–STAT1 signaling or mTORC1 activation (Fig. 6A, Supplementary Fig. 6A).
397 Similar results were observed using IFNβ (Supplementary Fig. 6B). Thus, type I IFN, in synergy
398 with anti-CD3/anti-CD28, promoted p-AKT_{473} in a RICTOR dependent manner. We also
399 observed similar synergy between TCR and type I IFN on mTORC2 activation in human $CD4^+$ T
400 cells (Fig. 6C). Type I IFN is known to suppress lymphocyte egress from lymph nodes to blood,

401 partly through induction of CD69 expression[7,8]. Poly(I:C) is a potent inducer of type I IFN. It
402 induces $CD4^+$ T cell lymphopenia in an IFNAR dependent manner[8]. Indeed, administering
403 poly(I:C) induced potent CD69 expression on blood $CD4^+$ T cell (Fig. 6D), and induced $CD4^+$ T
404 cell lymphopenia (Fig. 6E). Both phenotypes were significantly reversed in $CD4^+$ T cells from
405 *Cd4*^{Cre}*Rictor*$^{fl/fl}$ mice. Such phenotype was not observed in $CD19^+$ B cells, in which RICTOR
406 was intact (Supplemental Fig. 6C), indicating that type I IFN promotes $CD4^+$ T cell lymphopenia
407 partly through T cell intrinsic mTORC2. Consistent with these observations, Lpr $CD4^+$ T cells
408 had increased CD69 level, which was restored in Lpr.*Rictor* T-KO mice in both lymph nodes and
409 blood (Fig. 6F, Supplemental Fig. 6D). Importantly, the severe $CD4^+$ T cell lymphopenia
410 phenotype in Lpr mice was also modestly, but significantly, reversed by RICTOR deficiency
411 (Fig. 6G, Supplemental Fig. 6E). The rescue effect on CD69 expression was consistently more
412 pronounced than that on $CD4^+$ T cell lymphopenia (Fig. 6D-G), suggesting that a large part of
413 lymphopenia phenotype in Lpr mice may be CD69 independent. Altogether, $CD4^+$ T cells from
414 Lpr mice exhibited increased mTORC2 activity. Type I IFN, together with TCR signaling,
415 activates mTORC2 to induce CD69 expression on $CD4^+$ T cells and blocks $CD4^+$ T cell egress
416 into blood. RICTOR deficiency partially restores $CD4^+$ T cell lymphopenia in Lpr mice.
417

418 **DISCUSSION**

419 In this study, we experimentally tested the hypothesis that genetic targeting mTORC2 in T cells
420 may benefit systemic autoimmunity using a classic systemic lymphoproliferative mouse model,
421 Lpr mice. We made several key observations: 1) T cells in Lpr mice have elevated mTORC2
422 activity and mTORC2 inhibition through genetic deletion of RICTOR in T cells can significantly
423 ameliorate immunopathology of Lpr mice, including increased GC B cells and extrafollicular B

424 cells; 2) RICTOR deficiency restores Tfh and Treg balance in Lpr mice, without significant
425 alteration of T cell proliferation and Th1 and Th17 lineages; 3) RICTOR deficiency in Tregs
426 fails to rectify most of the lymphoproliferative phenotypes in Lpr mice; 4) RICTOR deficiency
427 reduces ICOS-mediated glycolysis in Lpr T cells. 5) Type I IFN promotes mTORC2 activation
428 in $CD4^+$ T cells partly to drive CD69 expression and T cell lymphopenia. Thus, our study
429 suggests that mTORC2 might be a potential therapeutic target for systemic autoimmunity.
430
431 Our genetic studies demonstrated that mTORC2-dependent overactivation of Tfh cells, but not
432 impairment of Tregs, contributes to systemic autoimmunity in Lpr mice. Although previous
433 study showed deletion of *Rictor* in Tregs restores Treg suppressive activity, including the Tfh
434 suppressing ability, our data demonstrated that deletion of mTORC2 in Tregs does not improve
435 their ability to suppress Tfh cells in Lpr mice. These observations suggest that the ability to
436 promote Tfh differentiation is likely a more dominant function of mTORC2 in systemic
437 autoimmunity, at least in Lpr background. Furthermore, it is worth noting that while RICTOR
438 deficiency greatly reduced Tfh differentiation in Lpr mice, it did not significantly affect Th1 and
439 Th17 subsets, T cell IL-2 production and proliferation. These observations are consistent with
440 our hypothesis that mTORC2 specifically promotes Tfh differentiation without substantial
441 effects on T cell activation, proliferation, and other effector T cell lineages. This contrasts with
442 mTORC1, which is required for T cell quiescence exit and all effector T cell lineages[22]. Thus,
443 our data suggest that targeting mTORC2 may specifically suppress Tfh lineage, which may have
444 relatively smaller immunosuppressive side effects, compared to inhibition of mTORC1.
445

446 It has long been established that exuberant type I IFN activity contributes to lupus development.
447 Yet, the molecular mechanism through which type I IFN impact T cells in lupus remains largely
448 unknown. We show that type I IFN may be one of the upstream signals that activate mTORC2 in
449 T cells. One of the downstream effects of type I IFN-mTORC2 activation is to promote CD69
450 expression and T cell lymphopenia. However, our data also showed that mTORC2 is only part of
451 type I IFN program that controls T cell egress, because RICTOR deficiency had a relatively
452 small rescue effect on poly(I:C) induced lymphopenia or lymphopenia in Lpr mice. The
453 prevailing theory on the pathogenesis of the lymphopenia in lupus has been centered on
454 antilymphocyte antibodies[51]. But a large-scale multiplex single cell RNA-seq analysis
455 demonstrated a clear inverse correlation between type I IFN activity and circulating naïve $CD4^+$
456 T cells in SLE patients[12]. Our study corroborates with such observation indicating that elevated
457 type I IFN production may be another contributing factor for the lymphopenia phenotype in
458 lupus partly by potentiating mTORC2 activation. Consistent with this idea, a recent clinical trial
459 showed that type I IFN receptor blockade can correct the T cell lymphopenia phenotype in
460 patients with SLE[52]. One major limitation of our study is that our conclusions are based on one
461 genetic mouse model, Lpr mice. Lpr mice carry spontaneous mutation in *Fas* gene. On C57BL/6
462 background, *Fas* mutation does not lead to full-blown clinical symptoms characteristic of human
463 SLE, although many of the immune cell hyperactivation phenotypes resemble SLE. Further
464 investigations using other mouse models and patient samples are needed. Altogether, our results
465 support the notion that mTORC2 could be a novel target for systemic autoimmunity.
466
467

468 **ACKNOWLEDGEMENTS**

469 We thank Drs. Virginia Shapiro and Jie Sun for thoughtful discussions. This work was partly
470 supported by NIH R01AR077518 and R01Al162678, Mayo Foundation for Medical Education
471 and Research, and Center for Biomedical Discovery at Mayo Clinic, and Lupus Research
472 Alliance (696599, to H.Z.).

473

474 **Author contributions**

475 H.Z. conceived and designed the study. X.Z. designed the experiments and performed most of
476 the *in vitro* and *in vivo* experiments. H.Q. and M.L. performed ELISA analyses and cellularity
477 calculations. Y.L. performed immunofluorescence assays on spleen samples. X.Z. performed
478 some of the immunoblot assays. S.A. and M.A. analyzed histological samples. C.D. and A.D.
479 performed immunofluorescence assays on kidney samples.

480

481

482 **Competing interests**

483 The authors declare no conflict of interests.

484

485

486

487

488

489

490 **REFERENCE**

491 1. Muskardin, T.L.W. & Niewold, T.B. Type I interferon in rheumatic diseases. *Nat Rev*
492 *Rheumatol* **14**, 214-228 (2018).
493 2. Banchereau, J. & Pascual, V. Type I interferon in systemic lupus erythematosus and other
494 autoimmune diseases. *Immunity* **25**, 383-392 (2006).
495 3. Liu, Z. & Davidson, A. Taming lupus-a new understanding of pathogenesis is leading to
496 clinical advances. *Nature medicine* **18**, 871-882 (2012).
497 4. Morand, E.F.*, et al.* Trial of Anifrolumab in Active Systemic Lupus Erythematosus. *The*
498 *New England journal of medicine* **382**, 211-221 (2020).
499 5. Klarquist, J.*, et al.* Type I IFN Drives Experimental Systemic Lupus Erythematosus by
500 Distinct Mechanisms in CD4 T Cells and B Cells. *Immunohorizons* **4**, 140-152 (2020).
501 6. Liu, Z.*, et al.* Interferon-alpha accelerates murine systemic lupus erythematosus in a T
502 cell-dependent manner. *Arthritis Rheum* **63**, 219-229 (2011).
503 7. Shiow, L.R.*, et al.* CD69 acts downstream of interferon-alpha/beta to inhibit S1P1 and
504 lymphocyte egress from lymphoid organs. *Nature* **440**, 540-544 (2006).
505 8. Kamphuis, E., Junt, T., Waibler, Z., Forster, R. & Kalinke, U. Type I interferons directly
506 regulate lymphocyte recirculation and cause transient blood lymphopenia. *Blood* **108**, 3253-3261
507 (2006).
508 9. Su, C.C., Shau, W.Y., Wang, C.R., Chuang, C.Y. & Chen, C.Y. CD69 to CD3 ratio of
509 peripheral blood mononuclear cells as a marker to monitor systemic lupus erythematosus disease
510 activity. *Lupus* **6**, 449-454 (1997).
511 10. Tsujimura, S., Adachi, T., Saito, K. & Tanaka, Y. Role of P-glycoprotein on
512 CD69(+)CD4(+) cells in the pathogenesis of proliferative lupus nephritis and non-responsiveness
513 to immunosuppressive therapy. *RMD Open* **3**, e000423 (2017).
514 11. Oke, V.*, et al.* High levels of circulating interferons type I, type II and type III associate
515 with distinct clinical features of active systemic lupus erythematosus. *Arthritis Res Ther* **21**, 107
516 (2019).
517 12. Perez, R.K.*, et al.* Single-cell RNA-seq reveals cell type-specific molecular and genetic
518 associations to lupus. *Science* **376**, eabf1970 (2022).
519 13. Mountz, J.D., Hsu, H.C. & Ballesteros-Tato, A. Dysregulation of T Follicular Helper
520 Cells in Lupus. *J Immunol* **202**, 1649-1658 (2019).
521 14. Choi, J.Y.*, et al.* Circulating follicular helper-like T cells in systemic lupus
522 erythematosus: association with disease activity. *Arthritis Rheumatol* **67**, 988-999 (2015).
523 15. Crotty, S. T Follicular Helper Cell Biology: A Decade of Discovery and Diseases.
524 *Immunity* **50**, 1132-1148 (2019).
525 16. Odegard, J.M.*, et al.* ICOS-dependent extrafollicular helper T cells elicit IgG production
526 via IL-21 in systemic autoimmunity. *J Exp Med* **205**, 2873-2886 (2008).
527 17. Poholek, A.C.*, et al.* In vivo regulation of Bcl6 and T follicular helper cell development.
528 *J Immunol* **185**, 313-326 (2010).
529 18. Lee, S.K.*, et al.* B cell priming for extrafollicular antibody responses requires Bcl-6
530 expression by T cells. *J Exp Med* **208**, 1377-1388 (2011).
531 19. Jenks, S.A., Cashman, K.S., Woodruff, M.C., Lee, F.E. & Sanz, I. Extrafollicular
532 responses in humans and SLE. *Immunol Rev* **288**, 136-148 (2019).
533 20. Mizui, M. & Tsokos, G.C. Targeting Regulatory T Cells to Treat Patients With Systemic
534 Lupus Erythematosus. *Front Immunol* **9**, 786 (2018).

535 21. Saxton, R.A. & Sabatini, D.M. mTOR Signaling in Growth, Metabolism, and Disease.
536 *Cell* **169**, 361-371 (2017).
537 22. Zeng, H. & Chi, H. mTOR signaling in the differentiation and function of regulatory and
538 effector T cells. *Curr Opin Immunol* **46**, 103-111 (2017).
539 23. Hao, Y.*, et al.* The Kinase Complex mTOR Complex 2 Promotes the Follicular Migration
540 and Functional Maturation of Differentiated Follicular Helper CD4(+) T Cells During Viral
541 Infection. *Front Immunol* **9**, 1127 (2018).
542 24. Zeng, H.*, et al.* mTORC1 and mTORC2 Kinase Signaling and Glucose Metabolism Drive
543 Follicular Helper T Cell Differentiation. *Immunity* **45**, 540-554 (2016).
544 25. Zeng, H.*, et al.* mTORC1 couples immune signals and metabolic programming to
545 establish T(reg)-cell function. *Nature* **499**, 485-490 (2013).
546 26. Shi, H.*, et al.* Amino Acids License Kinase mTORC1 Activity and Treg Cell Function
547 via Small G Proteins Rag and Rheb. *Immunity* **51**, 1012-1027 e1017 (2019).
548 27. Chapman, N.M.*, et al.* mTOR coordinates transcriptional programs and mitochondrial
549 metabolism of activated Treg subsets to protect tissue homeostasis. *Nat Commun* **9**, 2095 (2018).
550 28. Hosokawa, T.*, et al.* Lamtor1 Is Critically Required for CD4(+) T Cell Proliferation and
551 Regulatory T Cell Suppressive Function. *J Immunol* **199**, 2008-2019 (2017).
552 29. Shrestha, S.*, et al.* Treg cells require the phosphatase PTEN to restrain TH1 and TFH cell
553 responses. *Nat Immunol* **16**, 178-187 (2015).
554 30. Huynh, A.*, et al.* Control of PI(3) kinase in Treg cells maintains homeostasis and lineage
555 stability. *Nat Immunol* **16**, 188-196 (2015).
556 31. Charbonnier, L.M.*, et al.* Functional reprogramming of regulatory T cells in the absence
557 of Foxp3. *Nat Immunol* **20**, 1208-1219 (2019).
558 32. Wyman, B. & Perl, A. Metabolic pathways mediate pathogenesis and offer targets for
559 treatment in rheumatic diseases. *Curr Opin Rheumatol* **32**, 184-191 (2020).
560 33. Suarez-Fueyo, A., Barber, D.F., Martinez-Ara, J., Zea-Mendoza, A.C. & Carrera, A.C.
561 Enhanced phosphoinositide 3-kinase delta activity is a frequent event in systemic lupus
562 erythematosus that confers resistance to activation-induced T cell death. *J Immunol* **187**, 2376-
563 2385 (2011).
564 34. Kato, H. & Perl, A. Blockade of Treg Cell Differentiation and Function by the
565 Interleukin-21-Mechanistic Target of Rapamycin Axis Via Suppression of Autophagy in Patients
566 With Systemic Lupus Erythematosus. *Arthritis Rheumatol* **70**, 427-438 (2018).
567 35. Li, W., Titov, A.A. & Morel, L. An update on lupus animal models. *Curr Opin*
568 *Rheumatol* **29**, 434-441 (2017).
569 36. Lee, K.*, et al.* Mammalian target of rapamycin protein complex 2 regulates differentiation
570 of Th1 and Th2 cell subsets via distinct signaling pathways. *Immunity* **32**, 743-753 (2010).
571 37. Delgoffe, G.M.*, et al.* The kinase mTOR regulates the differentiation of helper T cells
572 through the selective activation of signaling by mTORC1 and mTORC2. *Nat Immunol* **12**, 295-
573 303 (2011).
574 38. Kelley, V.E. & Roths, J.B. Interaction of mutant lpr gene with background strain
575 influences renal disease. *Clin Immunol Immunopathol* **37**, 220-229 (1985).
576 39. Chen, L.*, et al.* CD38-Mediated Immunosuppression as a Mechanism of Tumor Cell
577 Escape from PD-1/PD-L1 Blockade. *Cancer Discov* **8**, 1156-1175 (2018).
578 40. Clement, R.L.*, et al.* Follicular regulatory T cells control humoral and allergic immunity
579 by restraining early B cell responses. *Nat. Immunol.* **20**, 1360-1371 (2019).

580 41. Yang, J., *et al.* Critical roles of mTOR Complex 1 and 2 for T follicular helper cell
581 differentiation and germinal center responses. *Elife* **5**(2016).
582 42. Morel, L. Immunometabolism in systemic lupus erythematosus. *Nat Rev Rheumatol* **13**,
583 280-290 (2017).
584 43. Yin, Y., *et al.* Glucose Oxidation Is Critical for CD4+ T Cell Activation in a Mouse
585 Model of Systemic Lupus Erythematosus. *J Immunol* **196**, 80-90 (2016).
586 44. Yin, Y., *et al.* Normalization of CD4+ T cell metabolism reverses lupus. *Sci Transl Med*
587 **7**, 274ra218 (2015).
588 45. Frauwirth, K.A., *et al.* The CD28 signaling pathway regulates glucose metabolism.
589 *Immunity* **16**, 769-777 (2002).
590 46. Zheng, Y., Delgoffe, G.M., Meyer, C.F., Chan, W. & Powell, J.D. Anergic T cells are
591 metabolically anergic. *J. Immunol.* **183**, 6095-6101 (2009).
592 47. Kalekar, L.A., *et al.* CD4(+) T cell anergy prevents autoimmunity and generates
593 regulatory T cell precursors. *Nat Immunol* **17**, 304-314 (2016).
594 48. Xie, D.L., Wu, J., Lou, Y.L. & Zhong, X.P. Tumor suppressor TSC1 is critical for T-cell
595 anergy. *Proc Natl Acad Sci U S A* **109**, 14152-14157 (2012).
596 49. Braun, D., Geraldes, P. & Demengeot, J. Type I Interferon controls the onset and severity
597 of autoimmune manifestations in lpr mice. *Journal of autoimmunity* **20**, 15-25 (2003).
598 50. Nickerson, K.M., Cullen, J.L., Kashgarian, M. & Shlomchik, M.J. Exacerbated
599 autoimmunity in the absence of TLR9 in MRL.Fas(lpr) mice depends on Ifnar1. *J Immunol* **190**,
600 3889-3894 (2013).
601 51. Fayyaz, A., *et al.* Haematological manifestations of lupus. *Lupus Sci Med* **2**, e000078
602 (2015).
603 52. Casey, K.A., *et al.* Type I interferon receptor blockade with anifrolumab corrects innate
604 and adaptive immune perturbations of SLE. *Lupus Sci Med* **5**, e000286 (2018).
605

606 **FIGURE LEGENDS**

607 **Figure 1. *Rictor* deletion in T cells rectifies immunopathology in Lpr mice.** (A) Immunoblot
608 analysis of p-AKT473 in B6 and Lpr $CD4^+$ T cells isolated from peripheral lymph nodes (pLN).
609 Right, summary of the relative p-AKT473 expression (normalized to that in B6 $CD4^+$ T cells).
610 (B) Image of peripheral lymph nodes taken from 6 months old B6, Lpr and Lpr.*Rictor* T-KO
611 mice. Right, summary of total cellularity of lymph nodes. (C) Titers of total immunoglobulin (Ig)
612 M, IgG, IgG2b and IgG3 were measured by ELISA. (D) Titers of anti-ssDNA (left) and anti-
613 chromatin (right) were measured by ELISA. Samples were from 9 months old B6, Lpr and
614 Lpr.*Rictor* T-KO mice. (E) Expression of B220 and TCRβ on lymphocytes. Right, the
615 frequencies (upper panels) and absolute numbers (lower panels) of $B220^+TCR\beta^+$, $B220^-TCR\beta^+$,
616 $B220^+TCR\beta^-$ cells. (F) Flow cytometry analysis of CD4 and CD8 T cells among $B220^-TCR\beta^+$
617 cells. Right, the frequency (left) and absolute number (right) of $CD4^-CD8^-$ T cell population. (E)
618 and (F) Cells were from peripheral lymph nodes (pLN) of 6 months old B6, Lpr and Lpr.*Rictor*
619 T-KO mice. (G) The inflammatory cytokine levels in mouse sera samples collected from 5-6
620 months old B6, Lpr and Lpr.*Rictor* T-KO mice. NS, not significant; * $P < 0.05$, ** $P < 0.01$, ***
621 $P < 0.001$, **** $P < 0.0001$. *p* values were calculated with one-way ANOVA. Results were
622 presentative of 3 (A) independent experiment and pooled from at least 3 (A-G) independent
623 experiments. Error bars represent SEM.

624 **Figure 2. mTORC2 in T cells is required for B cell hyper-activation in Lpr mice.** (A)
625 Immunofluorescence staining of peanut agglutinin (PNA), CD3 and IgD on spleen sections from
626 6 months old B6, Lpr and Lpr.*Rictor* T-KO mice. (B) Flow cytometry analysis of GL-7 and IgD
627 expression among $B220^+TCR\beta^-$ cells. Right, the frequency of $IgD^-GL\text{-}7^+$ germinal center (GC)
628 B cells. (C) Immunofluorescence staining of CD138 and IgD on spleen sections from 6 months

629 old B6, Lpr and Lpr.*Rictor* T-KO mice. (D) Flow cytometry analysis of $B220^{+}CD138^{int}$ and
630 $B220^{lo}CD138^{hi}$ two populations. Right, the frequencies of $B220^{+}CD138^{int}$ (left) and
631 $B220^{lo}CD138^{hi}$ (right) among total lymphocytes. (B) and (D) Cells were from pLNs of 6 months
632 old B6, Lpr and Lpr.*Rictor* T-KO mice. NS, not significant; *** $P < 0.001$, **** $P < 0.0001$
633 (one-way ANOVA). Results were pooled from 3 (B and D) independent experiments. Error bars
634 represent SEM.

635 **Figure 3. *Rictor* deletion reduces Tfh differentiation, normalizes Treg frequencies, but does**
636 **not affect Th1 and Th17 differentiation or T cell proliferation.** (A) Expression of CXCR5
637 and BCL6 on $B220^{-}CD4^{+}$ T cells. Right, the percentages (left) and absolute numbers (right) of
638 $BCL6^{+}CXCR5^{+}$ and $BCL6^{-}CXCR5^{+}$ cells. (B) Expression of PSGL1 and CXCR5 on $B220^{-}$
639 $CD4^{+}$ T cells. Right, the summary of $PSGL1^{lo}CXCR5^{lo}$ extrafollicular (EF) Tfh cell percentages.
640 (C) Expression of ICOS on $B220^{-}CD4^{+}$ T cells. Right, the summary of $ICOS^{+}$ cell frequency
641 (left) and normalized ICOS median fluorescence intensity (MFI) (right). (D) Flow cytometry
642 analysis of Treg cells ($B220^{-}CD4^{+}FOXP3^{++}$). Frequencies of $FOXP3^{+}$ cells in $CD4^{+}$ T cells from
643 spleen (left), pLN (middle) and Peyer's patches (PP) (right). (E) The ratio between Tfh and Treg
644 frequency (left) and the ratio between Tfh and Tfr frequency (right) in $CD4^{+}$ T cells from B6,
645 Lpr and Lpr.*Rictor* T-KO mice. (F) Expression of IFNγ and IL-17 in $CD4^{+}$ T cells activated by
646 PMA and ionomycin. Right, frequencies of $IFN\gamma^{+}$ cells and $IL\text{-}17^{+}$ cells. (G) Expression of IL-2
647 in $CD4^{+}$ T cells activated by PMA and ionomycin. Right, the frequency of $IL\text{-}2^{+}$ cell. (H)
648 Expression of Ki-67 in $CD4^{+}$ T cells from B6, Lpr and Lpr.*Rictor* T-KO mice. Right, the
649 summary of $Ki\text{-}67^{+}$ cell frequency. (A-C, and E-H) Cells were from pLNs of 6 months old B6,
650 Lpr and Lpr.*Rictor* T-KO mice. NS, not significant; * $P < 0.05$, ** $P < 0.01$, *** $P < 0.001$, ****

651 $P < 0.0001$ (one-way ANOVA). Results were pooled from at least 3 (A-H) independent
652 experiments. Error bars represent SEM.

653 **Figure 4. *Rictor* deletion in Treg is unable to restore immune dysregulation in Lpr mice.**
654 (A) Frequency of FOXP3$^+$ Treg cells in splenic CD4$^+$ T cells. (B) Image of peripheral lymph
655 nodes taken from 6 months old B6, Lpr, Lpr.*Rictor* T-KO mice and Lpr.*Rictor* Treg-KO. Right,
656 summary of total cellularity of lymph nodes. (C) Frequency of B220$^+$TCRβ$^+$ cells in pLN among
657 B6, Lpr, Lpr.*Rictor* T-KO mice and Lpr.*Rictor* Treg-KO. (D) Frequencies of pre-Tfh (BCL6$^-$
658 CXCR5$^+$) and Tfh (BCL6$^+$CXCR5$^+$) cells in pLN. (E) Frequency of GC B cells. (F) The ratio
659 between Tfh and Treg frequency in CD4$^+$ T cells from B6, Lpr, Lpr.R*ictor* T-KO and Lpr.*Rictor*
660 Treg-KO mice. (G) Serum concentrations of immunoglobulin IgG1, IgG2a, and IgG2b were
661 measured by LEGENDplex. NS, not significant; * $P < 0.05$, ** $P < 0.01$, *** $P < 0.001$, **** P
662 < 0.0001 (one-way ANOVA). Results were pooled from at least 3 (A-G) independent
663 experiments. Error bars represent SEM.

664 **Figure 5. mTORC2 supports TCR/ICOS mediated glucose metabolism in Lpr T cells.** (A)
665 The basal respiration and (B) basal extracellular acidification rate (ECAR) of CD4$^+$ T from 2-,
666 3-, and 9-months old mice cells under anti-CD3/anti-CD28 overnight activation, respectively.
667 (C) The ECAR of CD4$^+$ T cells followed by sequential anti-CD3/anti-CD28, and anti-CD3/anti-
668 ICOS stimulation measured by glycolytic rate assay. Cells were from pLNs of 6 months old B6,
669 Lpr and Lpr.*Rictor* T-KO mice. Right, summaries of basal glycolysis and compensatory
670 glycolysis. Rot, Rotenone; AA, Antimycin A; 2-DG, 2-deoxyglucose. NS, not significant; * $P <$
671 0.05, ** $P < 0.01$, *** $P < 0.001$, **** $P < 0.0001$ (one-way ANOVA). Results were
672 presentative of 2 (A-B) and 3 (C) independent experiments. Error bars represent SEM.

673 **Figure 6. Type I IFN synergizes with TCR to promote CD69 expression and suppress T cell**
674 **egress.** (A) Immunoblot analysis of p-AKT$_{473}$, AKT (pan), p-STAT1 and p-S6 in CD4^{+} T cells
675 from B6 and *Cd4*^{cre}*Rictor*$^{fl/fl}$ mice stimulated with or without anti-CD3/anti-CD28 in the presence
676 or absence of IFNα for 1 and 6 hours. Right, summaries of the relative p-AKT$_{473}$ expression
677 (normalized to total AKT and then compared with baseline B6 CD4^{+} T cells) stimulated for 6
678 hours. (B) Flow cytometry analysis of p-AKT$_{473}$ expression in CD4^{+} T cells treated with IFNα
679 alone, or in combination with anti-CD3/anti-CD28 overnight. Right, summary of the relative
680 pAKT$_{473}$ expression (normalized to that in B6 CD4^{+} T cells without any stimulation). (C)
681 Immunoblot analysis of p-AKT$_{473}$, AKT (pan), and p-STAT1 in human CD4^{+} T cells with or
682 without anti-CD3/anti-CD28 activation in presence or absence of human IFNα for 3 hours.
683 Right, summary of the relative p-AKT$_{473}$ expression normalized to total AKT and then compared
684 with baseline. (D) and (E) B6 and *Cd4*^{cre}*Rictor*$^{fl/fl}$ mice were administered with poly(I:C)
685 intraperitoneally. (D) Expression of CD69 in blood CD4^{+} T cells from B6 and *Cd4*^{cre}*Rictor*$^{fl/fl}$
686 mice after poly(I:C) administration. Numbers indicate the percentages of CD69^{+}CD4^{+} T cells.
687 Right, summary of CD69^{+} percentage in CD4^{+} T cells at baseline or treated with poly(I:C) for 16
688 h and 40 h. (E) Blood CD4^{+} T cell counts were determined before and after poly(I:C) treatment.
689 (F) Expression of CD69 in CD4^{+} T cells from B6, Lpr and Lpr.*Rictor* T-KO mice. Right,
690 summary of CD69^{+} percentages among pLN CD4^{+} T cells. (G) Blood CD4^{+} T cell counts were
691 determined in 4-6 months old B6, Lpr and Lpr.*Rictor* T-KO mice. NS, not significant; * $P <$
692 0.05, ** $P < 0.01$, *** $P < 0.001$, **** $P < 0.0001$ (A, B, D and E, unpaired Student's *t* test, C, F
693 and G, one-way ANOVA). Results were presentative of 4 (A, C), or pooled from at least 3 (A-G)
694 independent experiments. Error bars represent SEM.
695

Figure 1

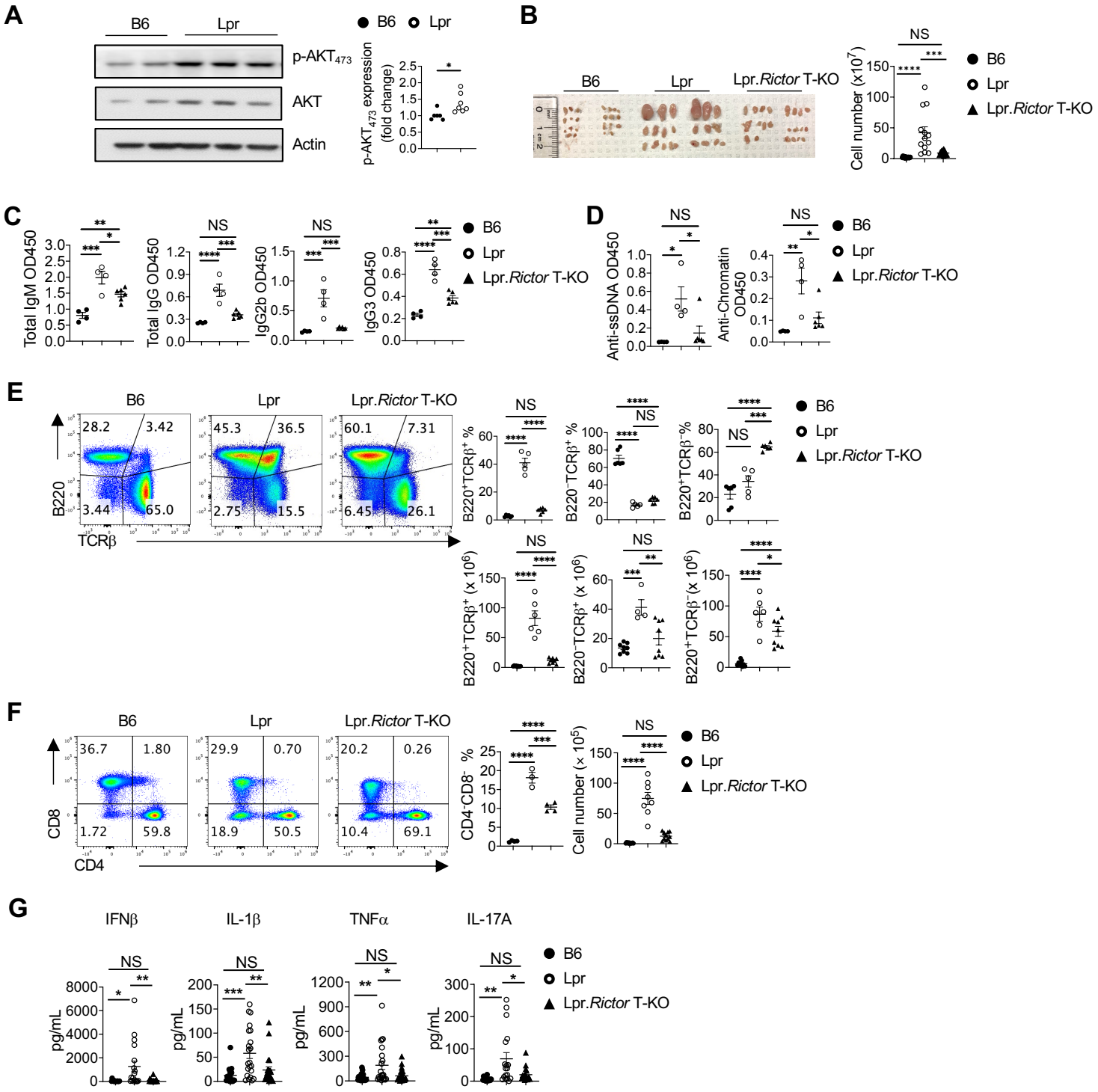
A
B6
Lpr
p-AKT473
AKT
Actin
p-AKT473 expression (fold change)
B
Lpr.Rictor T-KO
Cell number (x10^7)
NS
C
Total IgM OD450
Total IgG OD450
IgG2b OD450
IgG3 OD450
D
Anti-ssDNA OD450
Anti-Chromatin OD450
E
B220
TCRβ
B220+TCRβ+ %
B220-TCRβ+ %
B220+TCRβ- %
B220+TCRβ+ (x 10^6)
B220-TCRβ+ (x 10^6)
B220+TCRβ- (x 10^6)
F
CD8
CD4
CD4-CD8- %
Cell number (x 10^5)
G
IFNβ
IL-1β
TNFα
IL-17A
pg/mL

Figure 2

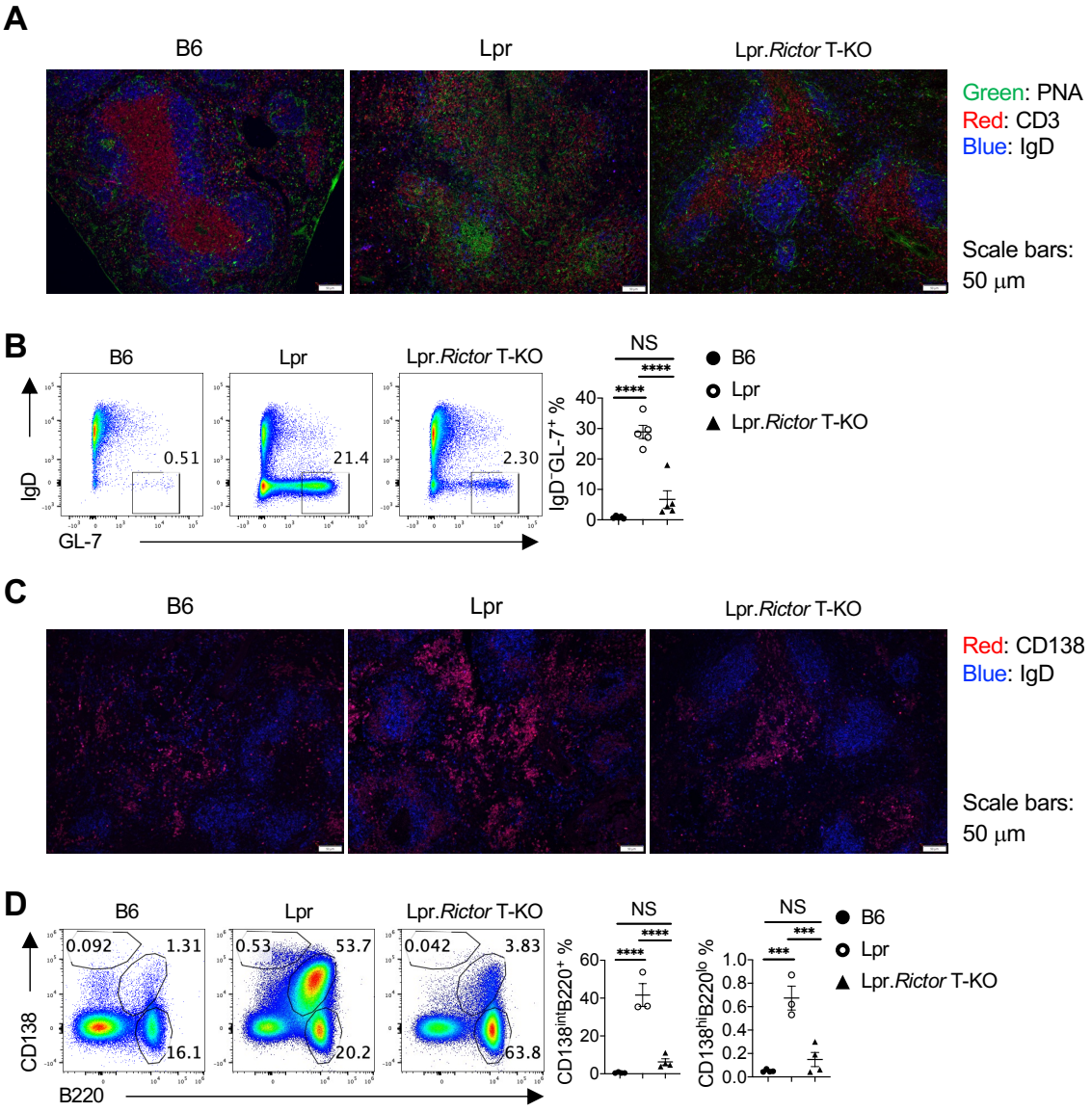
A
B6
Lpr
Lpr.Rictor T-KO
Green: PNA
Red: CD3
Blue: IgD
Scale bars:
50 μm
B
B6
Lpr
Lpr.Rictor T-KO
IgD
GL-7
0.51
21.4
2.30
NS
****
****
IgD⁻GL-7⁺ %
40
30
20
10
0
B6
Lpr
Lpr.Rictor T-KO
C
B6
Lpr
Lpr.Rictor T-KO
Red: CD138
Blue: IgD
Scale bars:
50 μm
D
B6
Lpr
Lpr.Rictor T-KO
CD138
B220
0.092
1.31
16.1
0.53
53.7
20.2
0.042
3.83
63.8
NS
****
****
CD138intB220+ %
60
40
20
0
NS
***
***
CD138hiB220lo %
1.0
0.8
0.6
0.4
0.2
0.0
B6
Lpr
Lpr.Rictor T-KO

Figure 3

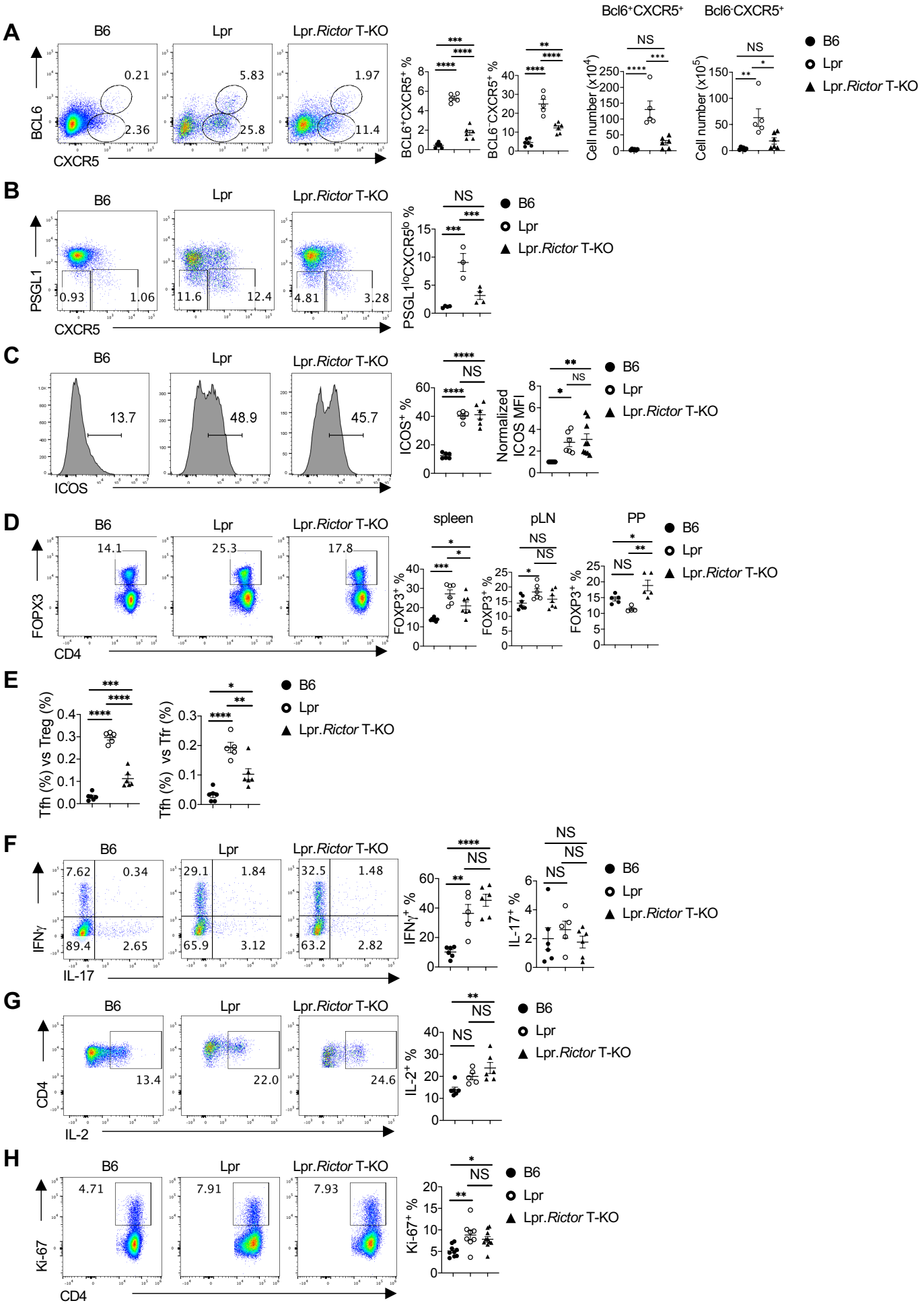
A
B6
Lpr
Lpr.Rictor T-KO
BCL6
CXCR5
0.21
2.36
5.83
25.8
1.97
11.4
Bcl6+CXCR5+
Bcl6-CXCR5+
BCL6+CXCR5+ %
BCL6-CXCR5+ %
Cell number (x10^4)
Cell number (x10^5)
NS
B
PSGL1
0.93
1.06
11.6
12.4
4.81
3.28
PSGL1loCXCR5lo %
C
ICOS
13.7
48.9
45.7
ICOS+ %
Normalized ICOS MFI
D
FOXP3
CD4
14.1
25.3
17.8
spleen
pLN
PP
FOXP3+ %
E
Tfh (%) vs Treg (%)
Tfh (%) vs Tfr (%)
F
IFNγ
IL-17
7.62
0.34
89.4
2.65
29.1
1.84
65.9
3.12
32.5
1.48
63.2
2.82
IFNγ+ %
IL-17+ %
G
IL-2
13.4
22.0
24.6
IL-2+ %
H
Ki-67
4.71
7.91
7.93
Ki-67+ %
B6
Lpr
Lpr.Rictor T-KO

Figure 4

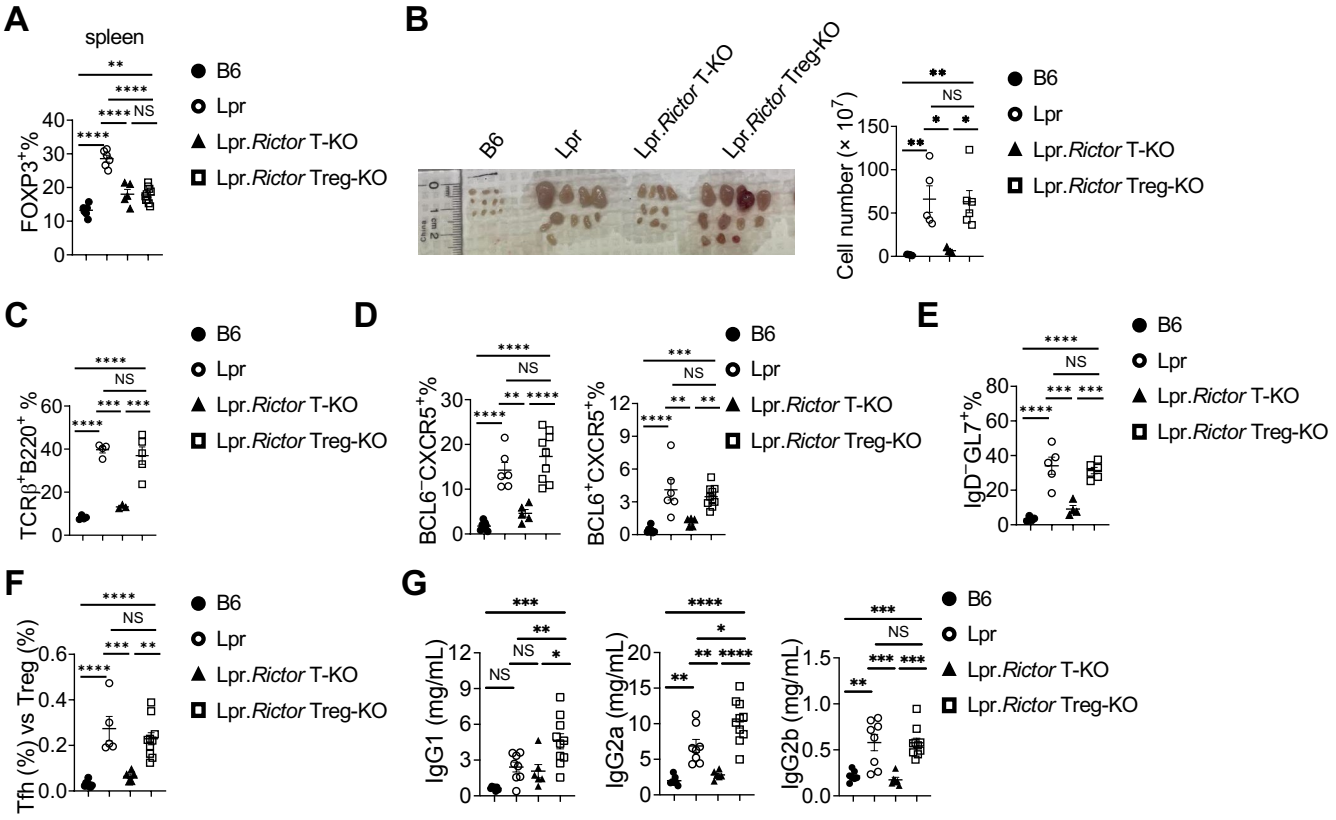
A
spleen
FOXP3+%
B6
Lpr
Lpr.Rictor T-KO
Lpr.Rictor Treg-KO
B
B6
Lpr
Lpr.Rictor T-KO
Lpr.Rictor Treg-KO
Cell number (× 10^7)
C
TCRβ+B220+ %
D
BCL6−CXCR5+%
BCL6+CXCR5+%
E
IgD−GL7+%
F
Tfh (%) vs Treg (%)
G
IgG1 (mg/mL)
IgG2a (mg/mL)
IgG2b (mg/mL)
NS

Figure 5

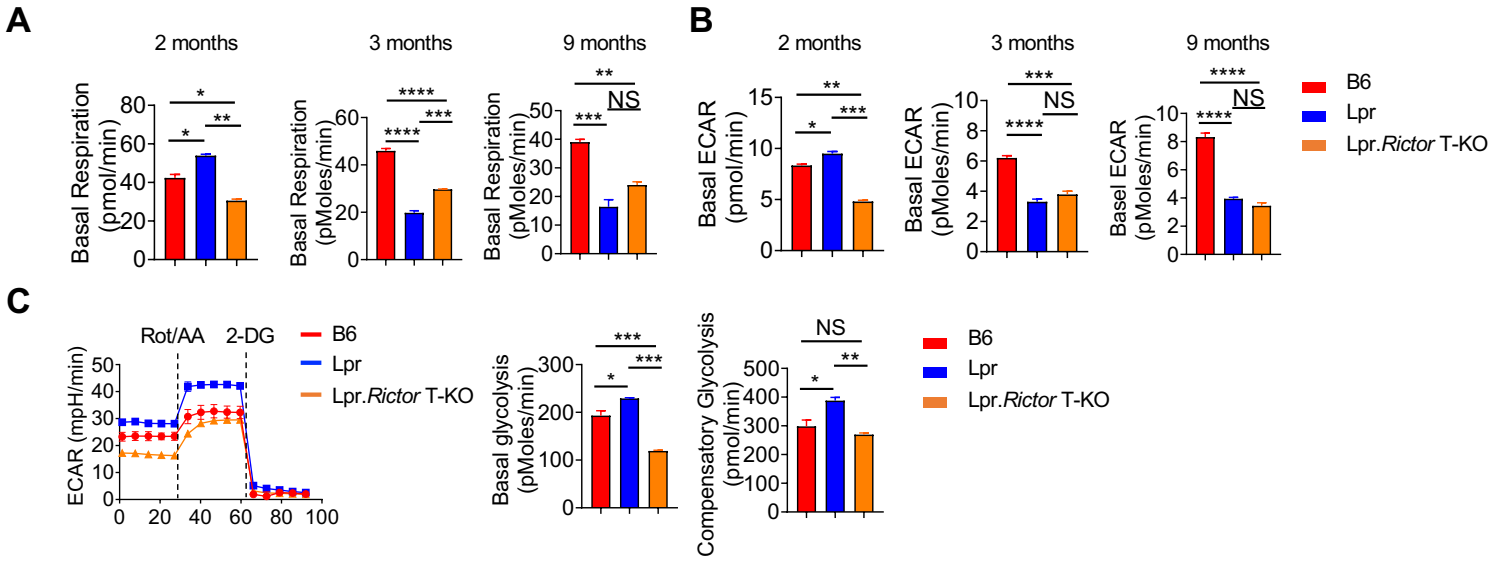
A
2 months
3 months
9 months
Basal Respiration (pmol/min)
Basal Respiration (pMoles/min)
Basal Respiration (pMoles/min)
B
Basal ECAR (pmol/min)
Basal ECAR (pMoles/min)
Basel ECAR (pMoles/min)
NS
B6
Lpr
Lpr.Rictor T-KO
C
Rot/AA
2-DG
ECAR (mpH/min)
Basal glycolysis (pMoles/min)
Compensatory Glycolysis (pmol/min)

Figure 6

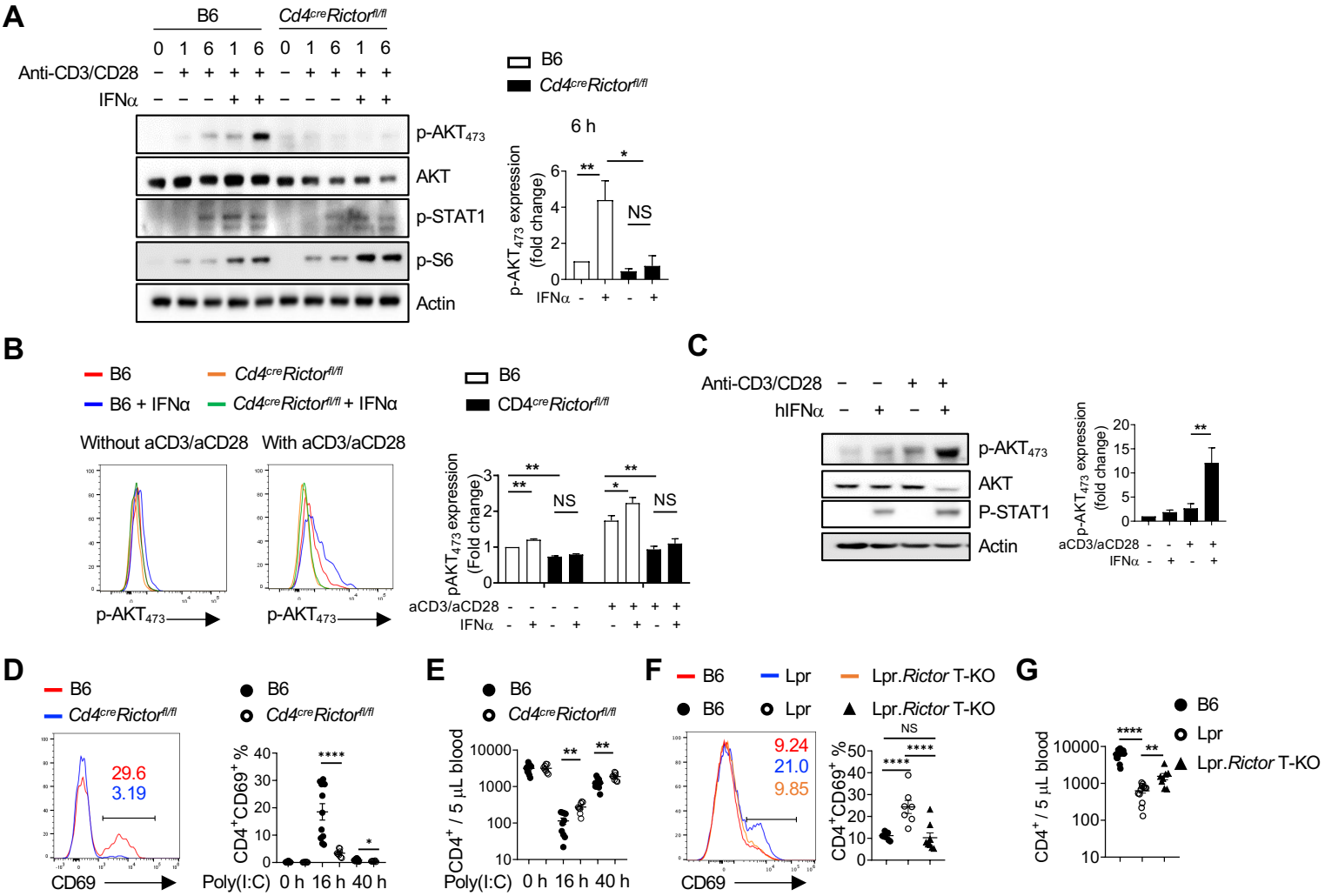
A
B6
Cd4creRictorfl/fl
0 1 6 1 6 0 1 6 1 6
Anti-CD3/CD28 − + + + + − + + + +
IFNα − − − + + − − − + +
p-AKT473
AKT
p-STAT1
p-S6
Actin
B6
Cd4creRictorfl/fl
6 h
p-AKT473 expression (fold change)
IFNα - + - +
B
B6
Cd4creRictorfl/fl
B6 + IFNα
Cd4creRictorfl/fl + IFNα
Without aCD3/aCD28
With aCD3/aCD28
p-AKT473
B6
CD4creRictorfl/fl
pAKT473 expression (Fold change)
aCD3/aCD28 - - - - + + + +
IFNα - + - + - + - +
NS
C
Anti-CD3/CD28 − − + +
hIFNα − + − +
p-AKT473
AKT
P-STAT1
Actin
p-AKT473 expression (fold change)
aCD3/aCD28 - - + +
IFNα - + - +
D
B6
Cd4creRictorfl/fl
29.6
3.19
CD69
CD4+CD69+ %
Poly(I:C) 0 h 16 h 40 h
E
B6
Cd4creRictorfl/fl
CD4+ / 5 µL blood
Poly(I:C) 0 h 16 h 40 h
F
B6
Lpr
Lpr.Rictor T-KO
9.24
21.0
9.85
CD69
CD4+CD69+ %
NS
G
B6
Lpr
Lpr.Rictor T-KO
CD4+ / 5 µL blood

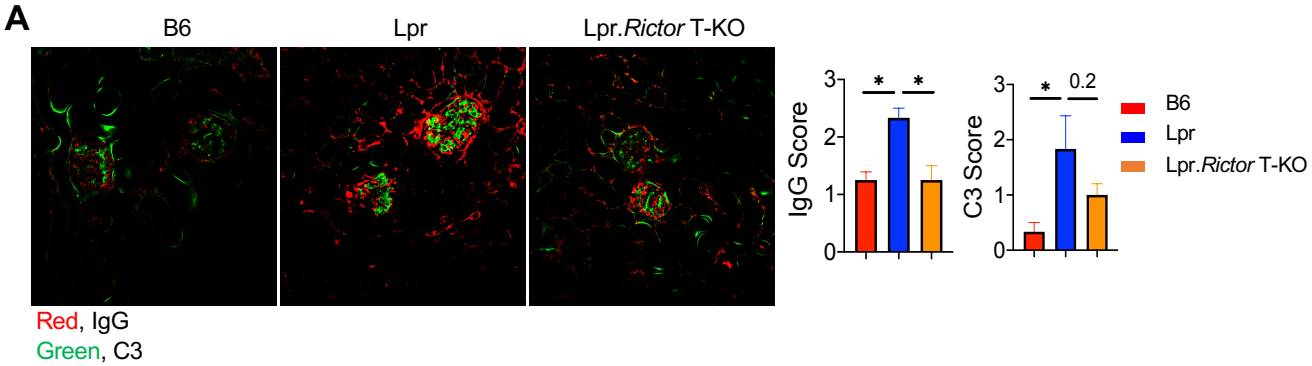

Supplemental Figure 1

(A) Immunofluorescence staining of IgG (Red) and C3 (Green) on mice kidney sections. Right, the scores of IgG and C3 deposition. * $P < 0.05$ (one-way ANOVA). Results were pooled from 2 independent experiments. Error bars represent SEM.

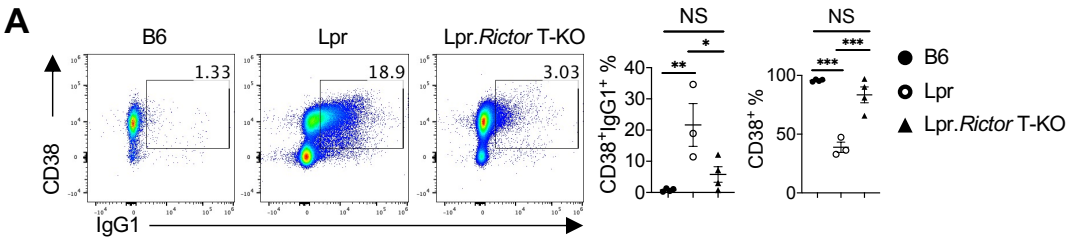

Supplemental Figure 2

(A) Expression of CD38 and IgG1 expression on B220^{+}TCRb^{-} B cells. Right, the frequencies of CD38^{+}IgG1^{+} B cells (left) and CD38^{+} percentages (right). (NS, not significant; * $P < 0.05$, ** $P < 0.01$, *** $P < 0.001$, **** $P < 0.0001$, one-way ANOVA, Results were pooled from 3 independent experiments. Error bars represent SEM.

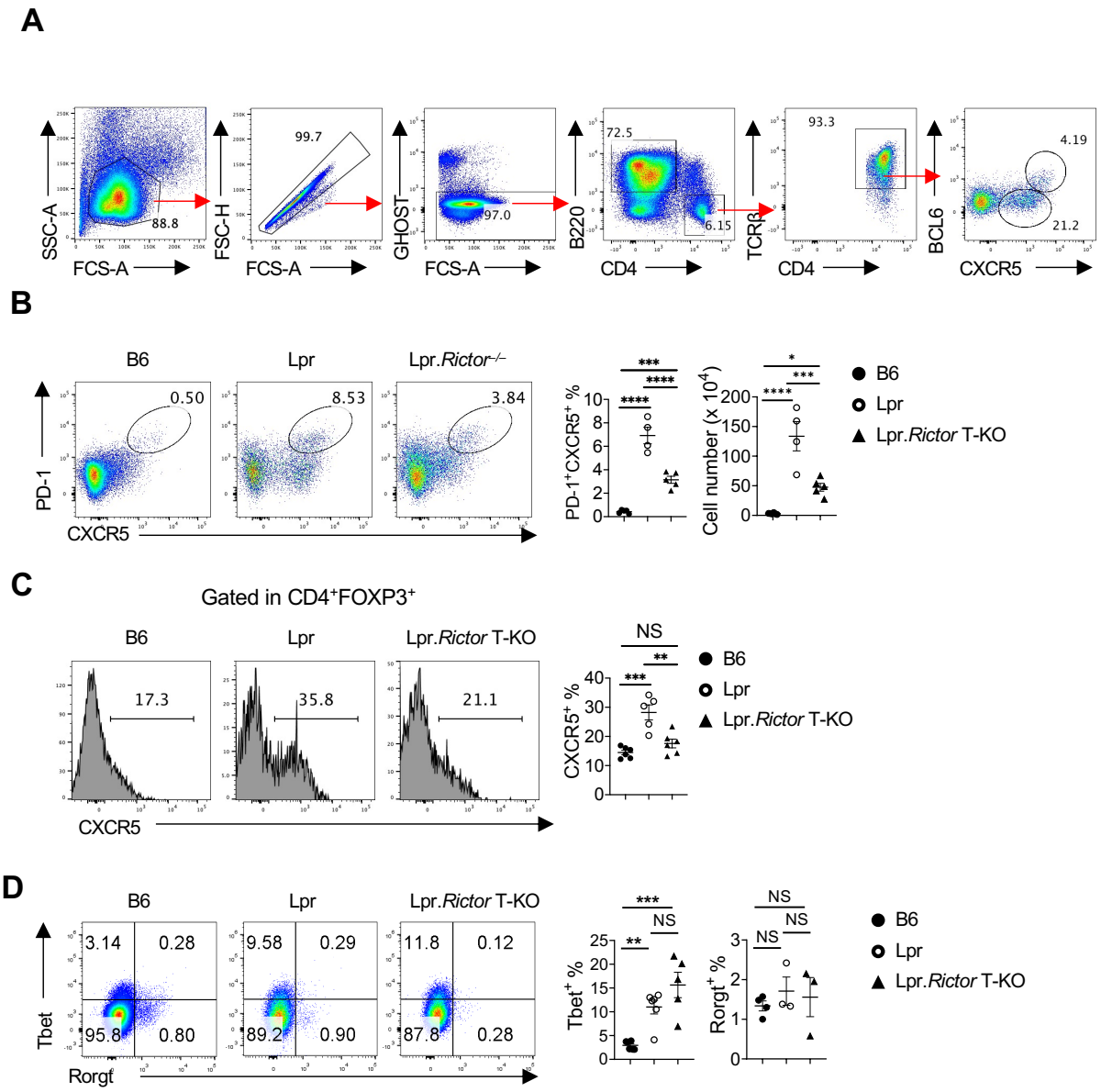

Supplemental Figure 3

(A) Gating strategy for analysis of Tfh cells.(B) Flow cytometry analysis of CXCR5 and PD-1 on B220^{-}CD4^{+} T cells. Right, the percentages of PD-1^{+}CXCR5^{+} cells. (C) Expression of CXCR5 in Tregs. Right, summary of CXCR5^{+} Tfr cell percentages. (D) Expression of CD25 on FOXP3^{+} Tregs. Numbers indicate the percentages of CD25^{-} Tregs. Right, summary of the percentages of CD25^{-} Tregs. (F) Expression of Tbet and Rorgt on on B220^{-}CD4^{+} T cells. Right, summary of Tbet^{+} and Rorgt^{+} cell percentages. Cells were from peripheral lymph nodes (pLNs) of 6 months old B6, Lpr and Lpr.*Rictor* T-KO mice. NS, not significant; ** $P < 0.01$, *** $P < 0.001$, **** $P < 0.0001$ (one-way ANOVA). Results were pooled from at least 3 independent experiments. Error bars represent SEM.

A

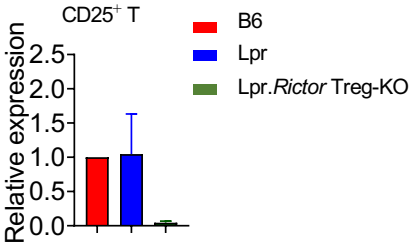

Supplemental Figure 4
(A) Expression of *Rictor* in sorted CD25$^+$ CD4$^+$ T cells from B6, Lpr, and Lpr.*Rictor* Treg-KO mice. Data represent 2 independent experiments.

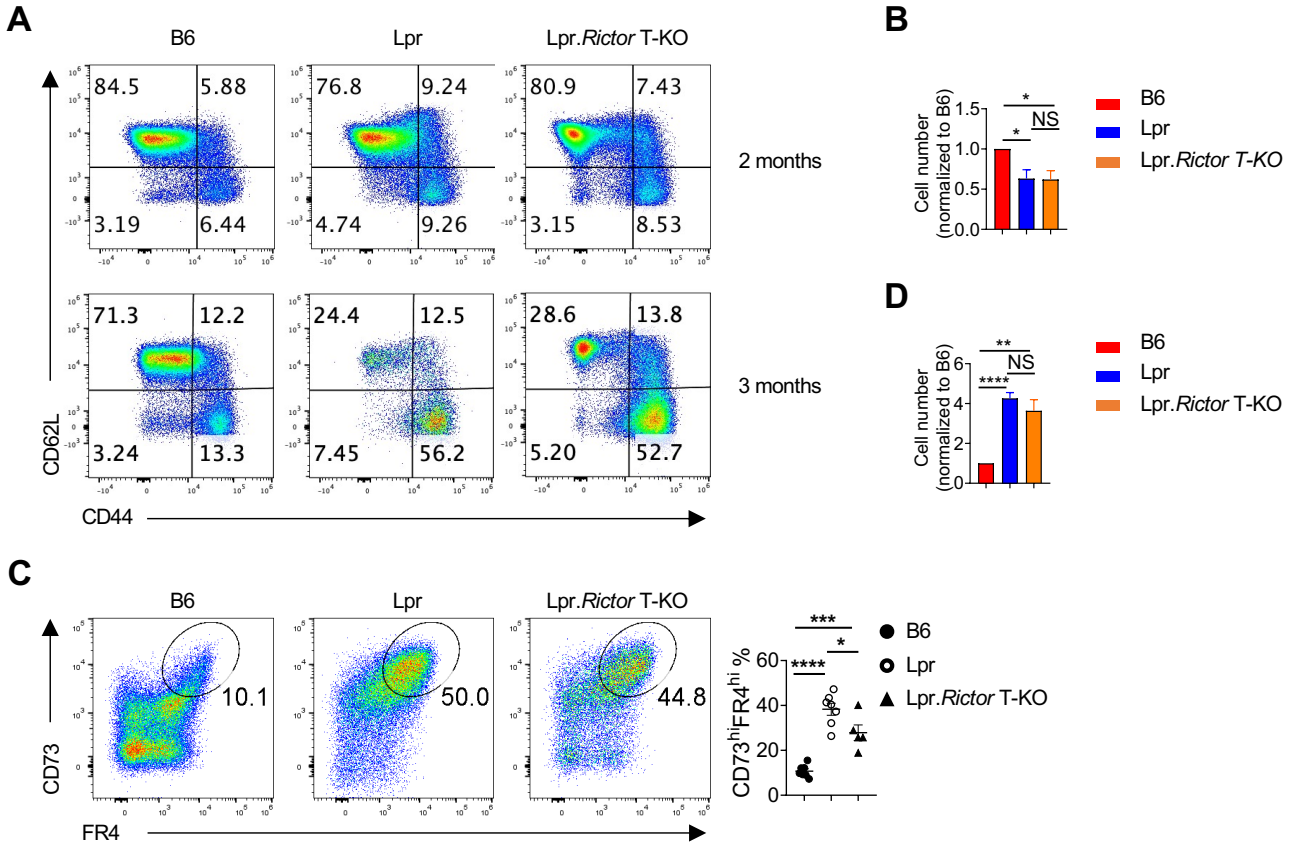

Supplemental Figure 5

(A) Flow cytometry analysis of CD44 vs. CD62L in B220^{-}CD4^{+} T cells among 2 and 3 months old B6, Lpr and Lpr.*Rictor* T-KO mice, respectively. (B) Summary of cell numbers for B220^{-}CD4^{+} T cells with anti-CD3/anti-CD28 activation for 72 hours. Numbers were normalized to B6 control. (C) Flow cytometry analysis of CD73 vs. FR4 expression in B220^{-}CD4^{+} T cells among 6 months old B6, Lpr and Lpr.*Rictor* T-KO mice. Right, summaries of frequencies of CD73^{hi}FR4^{hi} populations. (D) Summary of cell numbers for B220^{-}CD4^{+} T cells activated with anti-CD3/anti-CD28, and then with secondary anti-CD3/ICOS stimulation. Numbers were normalized to B6 control. NS, not significant; * $P < 0.05$, ** $P < 0.01$, *** $P < 0.001$, **** $P < 0.0001$ (one-way ANOVA). Results were pooled from at least 3 independent experiments. Error bars represent SEM.

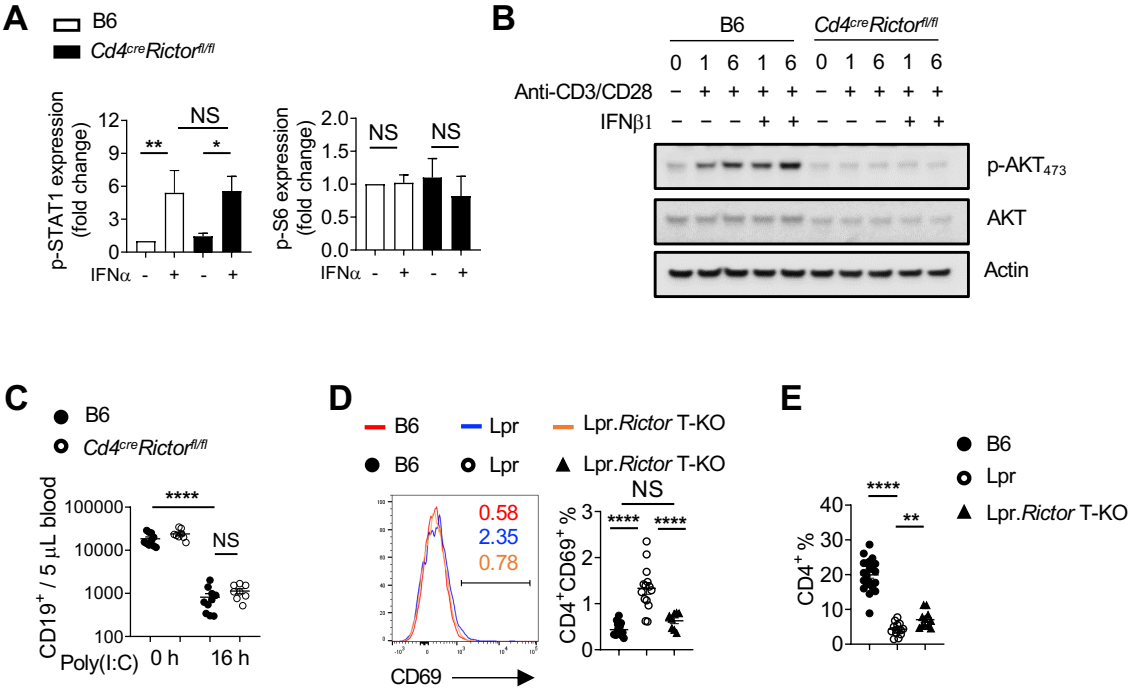

Supplemental Figure 6

(A) Immunoblot analysis of p-STAT1 and p-S6 expression in CD4$^+$ T cells from B6 and *Cd4^{cre}Rictor$^{fl/fl}$* mice treated with or without IFNα in presence of anti-CD3/anti-CD28 for 6 hours. The relative expressions were normalized to them in B6 CD4$^+$ T cells without any stimulation. (B) Immunoblot analysis of p-AKT473, p-STAT1 and Actin in CD4 T cells from B6 and *Cd4^{cre}Rictor$^{fl/fl}$* mice activated with anti-CD3/anti-CD28 in the presence or absence of IFNb. (C) Blood CD19$^+$ B cell counts were determined before and after poly(I:C) treatment in B6 and *Cd4^{cre}Rictor$^{fl/fl}$* mice. (D) Expression of CD69 was measured by flow cytometry in blood CD4$^+$ T cells from 4-6 months old B6, Lpr and Lpr.*Rictor* T-KO mice. Right, summary of CD69$^+$ percentages among blood CD4$^+$ T cells. (E) Percentages of CD19$^-$CD4$^+$ T cells in blood from B6, Lpr and Lpr.*Rictor* T-KO mice among total lymphocytes. NS, not significant; * $P < 0.05$, ** $P < 0.01$, *** $P < 0.001$, **** $P < 0.0001$ (A, unpaired Student's *t* test, C-E, one-way ANOVA). Results were pooled from at least 3 independent experiments. Error bars represent SEM.